JOURNAL OF COMPUTATIONAL PHYSICS 56, 287–323 (1984)

A Two-Dimensional Dispersion Analysis of Selected Methods for Solving the Linearized Shallow Water Equations

M. G. G. FOREMAN

Institute of Ocean Sciences, Sidney, British Columbia V8L 4B2, Canada

Received September 13, 1983

The accuracy and cost of three finite element methods for solving the linearized, two-dimensional shallow water equations are compared with a traditional explicit finite difference technique. Accuracy is determined by comparing numerical and analytic plane wave solutions. Cost is measured as the number of computations per unit of real time and per unit of model area. Two of the finite element methods are shown to be cost competitive, and as accurate as the chosen explicit finite difference technique. Though not comprehensive, the finite element analyses also suggest that meshes composed of equilateral triangles most accurately represent phase and group velocity.

INTRODUCTION

Within the last decade, finite element methods (FEMs) have become increasingly popular for solving the shallow water equations. Since they permit grids of variable size, shape, and orientation, they are usually able to provide a better approximation of the spatial domain than finite difference methods (FDMs). Specifically, better coastline fits are possible at model boundaries and grid size can be reduced in regions where the solution is expected to require greater resolution. However, most FEMs are not cost competitive with explicit FDMs. Their initialization costs and bookkeeping are more extensive, and more computations are usually required at each time step. For many applications this extra cost outweighs the advantages.

Some FEMs are able to significantly reduce their computations by "lumping" the matrix involved in the equation to be solved at each time step. Generally, lumping also reduces accuracy [13]. However, a recent study [3] of the one-dimensional "wave equation" FEM developed by Gray and Lynch [4, 11] demonstrates that with an appropriate choice of time stepping method, an accuracy loss need not occur.

In this discussion, three FEMs for solving the two-dimensional shallow water equations are compared with a traditional explicit FDM. The comparison is based on accuracy and cost. The analysis extends the one-dimensional techniques developed and illustrated in [2, 3].

Accuracy is measured by comparing numerical and analytic plane wave solutions. These calculations require simplifying the governing equations. Specifically, the equations are linearized, constant depth and a regular grid are assumed, and the

0021-9991/84 $3.00

complications of boundary conditions and initial conditions are ignored. Nevertheless, the performance of methods in such an idealized setting does give an indication of their accuracy in more complicated problems.

Cost is measured as the number of computations per unit of real time and per unit of model area. It ignores the model initialization. Using these measures, two of the FEMs are found to be cost competitive, and as accurate as the chosen explicit FDM.

This paper is divided into seven sections. Section 1 specifies the shallow water equations and their plane wave solutions, and defines concepts required in the subsequent analysis. Sections 2 through 5 examine the accuracy of specific methods with a Fourier or dispersion analysis which includes group velocity. Characteristic equations or dispersion relationships are calculated for all the numerical methods. From them, phase velocities, group velocities, and wave amplitude decay factors are then calculated and compared to the analytic values. Several diagrams facilitate the comparison.

Section 2 investigates the Richardson–Sielecki, [6, 1] FDM. It is a popular and successful explicit technique whose dispersion relationship has been previously calculated [12, 7].

Section 3 studies the Galerkin FEM with piecewise linear basis functions and Crank–Nicolson time stepping. The analysis is restricted to two combinations of six triangular elements. Since accuracy is dependent on the shape and configuration of the elements, this examination is meant to be illustrative rather than comprehensive. Nevertheless, one of the configurations is found to be more accurate and may well be optimal.

Section 4 studies Thacker's "irregular grid finite-difference" technique [20, 22]. For the chosen element configurations, it is simply a "lumped mass-matrix" version of the FEM in Section 3.

Section 5 studies the "wave equation" FEM and its lumped version. It extends the results of [3]. Section 6 assesses the cost and accuracy of the Richardson–Sielecki, Thacker, and lumped "wave equation" methods. Finally, Section 7 summarizes and briefly discusses the results.

1. Mathematic Background

The two-dimensional, linearized shallow water equations are

$$\frac{\partial z}{\partial t} + \frac{\partial (hu)}{\partial x} + \frac{\partial (hv)}{\partial y} = 0 \tag{1a}$$

$$\frac{\partial u}{\partial t} + g\frac{\partial z}{\partial x} - fv + \tau u = 0 \tag{1b}$$

$$\frac{\partial v}{\partial t} + g\frac{\partial z}{\partial y} + fu + \tau v = 0 \tag{1c}$$

where

$z(x, y, t)$ = elevation above mean sea level,

$u(x, y, t)$ = x component of the velocity,

$v(x, y, t)$ = y component of the velocity,

$h(x, y)$ = mean sea depth,

g = gravity,

$f(x, y)$ = Coriolis coefficient,

τ = linear bottom friction coefficient.

For the present analysis, the effects of both boundary conditions and initial conditions will be ignored.

Assuming constant values for the depth and Coriolis coefficient, plane wave solutions of the form

$$\begin{pmatrix} z(x, y, t) \\ u(x, y, t) \\ v(x, y, t) \end{pmatrix} = \mathrm{Re}\left\{ \begin{pmatrix} z_0 \\ u_0 \\ v_0 \end{pmatrix} \exp[i(k_1 x + k_2 y - \omega t)] \right\} \tag{2}$$

can be found for (1). ω is frequency and

$$\mathbf{k} = (k_1, k_2) \tag{3a}$$

are the (x, y) components of wavenumber. The distance between successive wave crests is the wavelength

$$L = 2\pi/k \tag{3b}$$

where

$$k = (k_1^2 + k_2^2)^{1/2}. \tag{3c}$$

For nontrivial solutions, the following cubic

$$\omega^3 + 2i\tau\omega^2 - \omega(\tau^2 + f^2 + ghk^2) - i\tau ghk^2 = 0 \tag{4}$$

must be satisfied. Dispersion relationships are obtained from its roots. Two cases are possible; either all three roots are purely imaginary, or one is purely imaginary and the other two, when multiplied by i, are complex conjugates [17]. The first case arises with relatively large τ and results in three stationary wave solutions. The complex conjugate roots in the second case are associated with gravity wave solutions that travel at the same speed in opposite directions, and have the same rates of amplitude decay (or growth). The third root would be associated with a planetary wave if either f or h were nonconstant [9]. However, when both are constant, as is assumed here,

this solution no longer propagates. It simply decays (or grows) in time. In the subsequent analysis, only numerical approximations to the gravity waves will be studied.

Phase and group velocity are defined [9] as

$$\mathbf{C} = \mathrm{Re}(\omega)\,\mathbf{k}/k^2 \tag{5a}$$

$$\mathbf{G} = \mathrm{Re}\left\{\left(\frac{\partial\omega}{\partial k_1}, \frac{\partial\omega}{\partial k_2}\right)\right\}. \tag{5b}$$

Whereas phase velocity describes the speed and direction of individual waves, group velocity describes the speed and direction of energy propagation. The importance of group velocity in numerical methods is surveyed by Trefethen [23]. Waves whose propagation speed $\mathbf{C}$ varies with the wavelength are said to be dispersive. If $\mathbf{C}$ is independent of direction, these waves are also said to be isotropic [10]. Although shallow water waves have virtually the same phase and group velocity, their numerical model representations may not.

2. The Richardson–Sielecki Finite Difference Scheme

A finite difference scheme which has been used successfully in many tide and storm surge problems [6, 1] is the Richardson–Sielecki (henceforth RS) scheme. It involves calculating variables on a Richardson grid [15] (also known as Arakawa's lattice C grid [12]) using a particular method of handling the Coriolis terms introduced by Sielecki [18]. Assuming a constant depth and Coriolis coefficient, its difference equations for solving (1) are

$$\frac{z_{rs}^{n+1} - z_{rs}^{n}}{\Delta t} + h\left(\frac{u_{r+1,s}^{n+1/2} - u_{rs}^{n+1/2}}{\Delta x} + \frac{v_{r,s+1}^{n+1/2} - v_{rs}^{n+1/2}}{\Delta y}\right) = 0 \tag{6a}$$

$$\frac{u_{rs}^{n+3/2} - u_{rs}^{n+1/2}}{\Delta t} + g\left(\frac{z_{rs}^{n+1} - z_{r-1,s}^{n+1}}{\Delta x}\right) - \frac{f}{4}\left(v_{r-1,s}^{n+1/2} + v_{rs}^{n+1/2} + v_{r-1,s+1}^{n+1/2} + v_{r,s+1}^{n+1/2}\right)$$
$$+ \tau(\theta u_{rs}^{n+3/2} + (1-\theta)\,u_{rs}^{n+1/2}) = 0 \tag{6b}$$

$$\frac{v_{rs}^{n+3/2} - v_{rs}^{n+1/2}}{\Delta t} + g\left(\frac{z_{rs}^{n+1} - z_{r,s-1}^{n+1}}{\Delta y}\right) + \frac{f}{4}\left(u_{rs}^{n+3/2} + u_{r,s-1}^{n+3/2} + u_{r+1,s}^{n+3/2} + u_{r+1,s-1}^{n+3/2}\right)$$
$$+ \tau(\theta v_{rs}^{n+3/2} + (1-\theta)\,v_{rs}^{n+1/2}) = 0. \tag{6c}$$

θ is a frictional weighting parameter and Δx, Δy, and Δt are the space and time step sizes. The elevation and velocity components are seen to be staggered by a half time step. The spatial placement of the variables is also staggered, as shown in Fig. 1. The scheme is explicit.

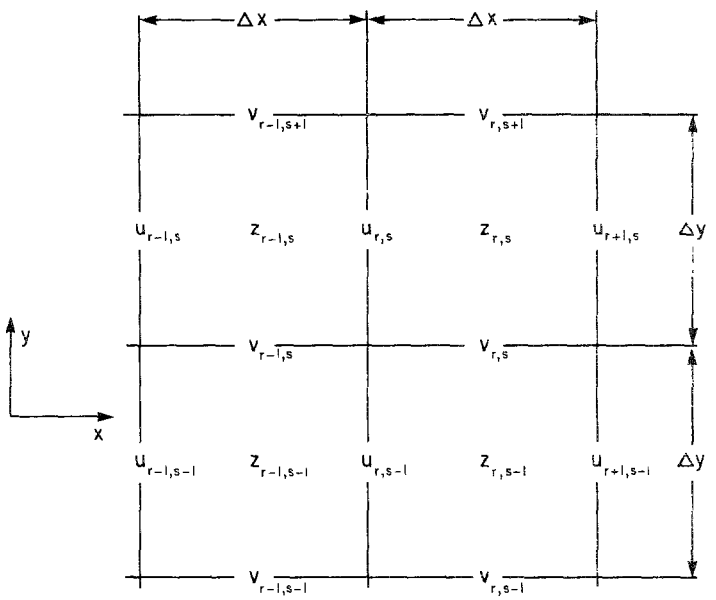

FIG. 1. Spatially discretized variables for the RS or lattice C grid.

The dispersion relationship for (6) is found by assuming the plane wave solutions

$$\begin{aligned} z_{rs}^{n} &= z_0 \exp[i(rk_1\,\Delta x + sk_2\,\Delta y - n\omega\,\Delta t)] \\ u_{rs}^{n+1/2} &= u_0 \exp[i(r-\tfrac{1}{2})\,k_1\,\Delta x + sk_2\,\Delta y - (n+\tfrac{1}{2})\,\omega\,\Delta t)] \\ v_{rs}^{n+1/2} &= v_0 \exp[i(rk_1\,\Delta x + (s-\tfrac{1}{2})\,k_2\,\Delta y - (n+\tfrac{1}{2})\,\omega\,\Delta t)]. \end{aligned} \tag{7}$$

A nontrivial solution requires

$$\begin{aligned} &(\lambda-1)\{[\lambda-1+\tau\,\Delta t(\theta\lambda+(1-\theta))]^2+\lambda[f\,\Delta t\cos(\tfrac{1}{2}k_1\,\Delta x)\cos(\tfrac{1}{2}k_2\,\Delta y)]^2\} \\ &\quad+4\lambda gh\,\Delta t^2[\lambda-1+\tau\,\Delta t(\theta\lambda+(1-\theta))]\left(\frac{\sin^2(\tfrac{1}{2}k_1\,\Delta x)}{(\Delta x)^2}+\frac{\sin^2(\tfrac{1}{2}k_2\,\Delta y)}{(\Delta y)^2}\right) \\ &\quad-\lambda(\lambda-1)\,gh\left(\frac{\Delta t^2}{\Delta x\,\Delta y}\right)\sin(k_1\,\Delta x)\sin(k_2\,\Delta y)f\,\Delta t=0 \end{aligned} \tag{8a}$$

where each root or eigenvalue can be expressed as

$$\lambda=\exp(-i\omega\,\Delta t). \tag{8b}$$

The frequencies ω may be complex.

For specific values of f, h, Δx, Δy, and τ, the roots of (8a) are functions of wavenumber. For $\tau=0$, these roots and the resultant dispersion relationship can be expressed algebraicly [7]. For nonzero τ, the result can be found numerically. In

particular, with $\Delta y = \Delta x$, $\omega \Delta t$ can be expressed in terms of the wavenumber sampling coordinates $(k_1 \Delta x, k_2 \Delta x)$ and the three parameters

$$f_1 = \tau \Delta x/(gh)^{1/2} \tag{9a}$$

$$f_2 = (gh)^{1/2} \Delta t/\Delta x \tag{9b}$$

$$f_3 = f \Delta x/(gh)^{1/2}. \tag{9c}$$

f_2 is commonly referred to as the Courant number while f_3 is a nondimensional inverse of the radius of deformation parameter used in [12]. f_1 and f_2 were parameters in [2].

Phase and group velocities for the RS scheme are calculated from the roots of (8) as

$$\mathbf{C}/(gh)^{1/2} = \frac{\mathrm{Re}(\omega \Delta t)}{f_2} \frac{(k_1 \Delta x, k_2 \Delta x)}{((k_1 \Delta x)^2 + (k_2 \Delta x)^2)} \tag{10a}$$

$$\mathbf{G}/(gh)^{1/2} = -\mathrm{Im}\left\{ \left(\frac{\partial \lambda}{\partial k_1 \Delta x}, \frac{\partial \lambda}{\partial k_2 \Delta x} \right) \Big/ (\lambda f_2) \right\}. \tag{10b}$$

An exhaustive comparison of the RS and analytic solutions will not be attempted here. Two roots of (8a) are associated with gravity waves. They will be studied in some detail. The third root will be considered only for its stability and its potential contamination of the gravity wave solution. Whereas $k_1 \Delta x$ and $k_2 \Delta x$ will vary over their complete domain $(-\pi, \pi]$, only a small portion of the (f_1, f_2, f_3, θ) parameter space will be examined. Subsequent figures for the RS scheme and the FEMs will be shown for $(f_1, f_3) = (0.05, 0.10)$. These are typical values for shallow water models at mid-latitudes. f_2 and time stepping parameters such as θ will have order unity $(O(1))$ or less, and will generally be chosen for high accuracy of the gravity wave solutions.

The RS dispersion surface for $\Delta y = \Delta x$ and $(f_1, f_2, f_3, \theta) = (0.05, 0.7071, 0.10, 0.5)$ is shown in Fig. 2. From (8a) it is seen that $(k_1 \Delta x, k_2 \Delta x)$ and $-(k_1 \Delta x, k_2 \Delta x)$ produce the same values. (This will be referred to as symmetry through the origin.) Hence only positive $k_2 \Delta x$ need be displayed. The "progressive wave" (positive ω) surface has been shown. A corresponding retrogressive surface (negative ω) exists and is simply the mirror image about the $(k_1 \Delta x, k_2 \Delta x)$ plane of the progressive surface. $f_2 = (2)^{-1/2}$ is the maximum permitted for stability when $\Delta y = \Delta x$ [7]. It is also the most accurate value for wave propagation in the $x = \pm y$ direction when $f = \tau = 0$.

The analytic dispersion surface has been included in Fig. 2 for comparison. As seen from (4), it is symmetric about both planes $k_1 = 0$ and $k_2 = 0$, and through the origin. Both the analytic and RS surfaces have maximum values of approximately $(2)^{1/2}$ at $(k_1 \Delta x/\pi, k_2 \Delta x/\pi) = (\pm 1, 1)$. It is the nonzero Coriolis parameter that gives the analytic surface a slight curvature.

Mesinger and Arakawa show $|\omega|/f$ contours for the spatially discretized RS scheme (the lattice C grid) with $f_3 = 0.5$. It has the same basic characteristics as

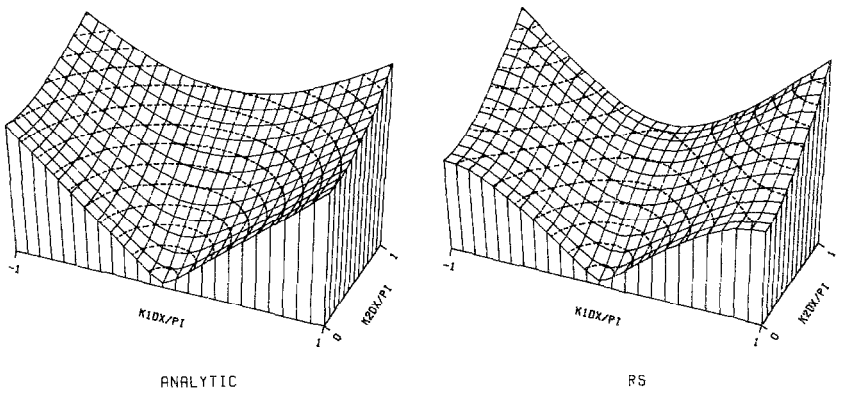

FIG. 2. Analytic and RS dispersion surfaces ($|\omega|\,\Delta x/(\pi(gh)^{1/2})$) for the parameter values $f_1 = 0.05$. $f_2 = 0.7071$, $f_3 = 0.10$. $\theta = 0.5$ and $\Delta x = \Delta y$ for the RS scheme. Dotted line contours are in increments of 0.10.

Fig. 2. Notice that for small wavenumber and $k_1 \simeq k_2$. RS surface values closely approximate the analytic.

Figure 3 displays the accuracy of the RS scheme. It plots the two accuracy measure functions

$$M_A = \left| \frac{\lambda_n}{\lambda_a} \right| \tag{11a}$$

$$M_C = \frac{|\mathbf{C}_n| - |\mathbf{C}_a|}{|\mathbf{C}_a|} \tag{11b}$$

where λ_n is the principal progressive numerical eigenvalue, λ_a is the analytic progressive eigenvalue, and $\mathbf{C}_n$, $\mathbf{C}_a$ are the corresponding phase velocities. Normalized group velocity vectors for both the analytic and RS solutions are also shown.

M_C is the relative error in phase velocity magnitude. Since it is calculated as a function of $\mathbf{k}$, it also equals the relative error in the frequency ω. Negative values denote waves travelling too slowly while zero values are optimal. For example, -0.01 denotes a numerical wave speed which is 1% too slow. The amplitude measure, M_A, is a ratio denoting the growth (or decay) factor per time step relative to the analytic solution. Values greater than the optimum of 1. signify a solution which decays too slowly or grows too rapidly. After n time steps, the ratio of the numerical amplitude to the analytic is $(M_A)^n$.

Wave amplitudes are seen to be accurately represented by the RS scheme. However, waves travelling to the north-east will be slightly too large while those to the north-west will be slightly too small. This effect is solely due to the asymmetric treatment of the Coriolis terms in (6). Specifically, when $f_3 = 0$, both M_A and M_C become symmetric about $k_1 = 0$. Henry [7] discusses alternative treatments of the Coriolis term which improve accuracy.

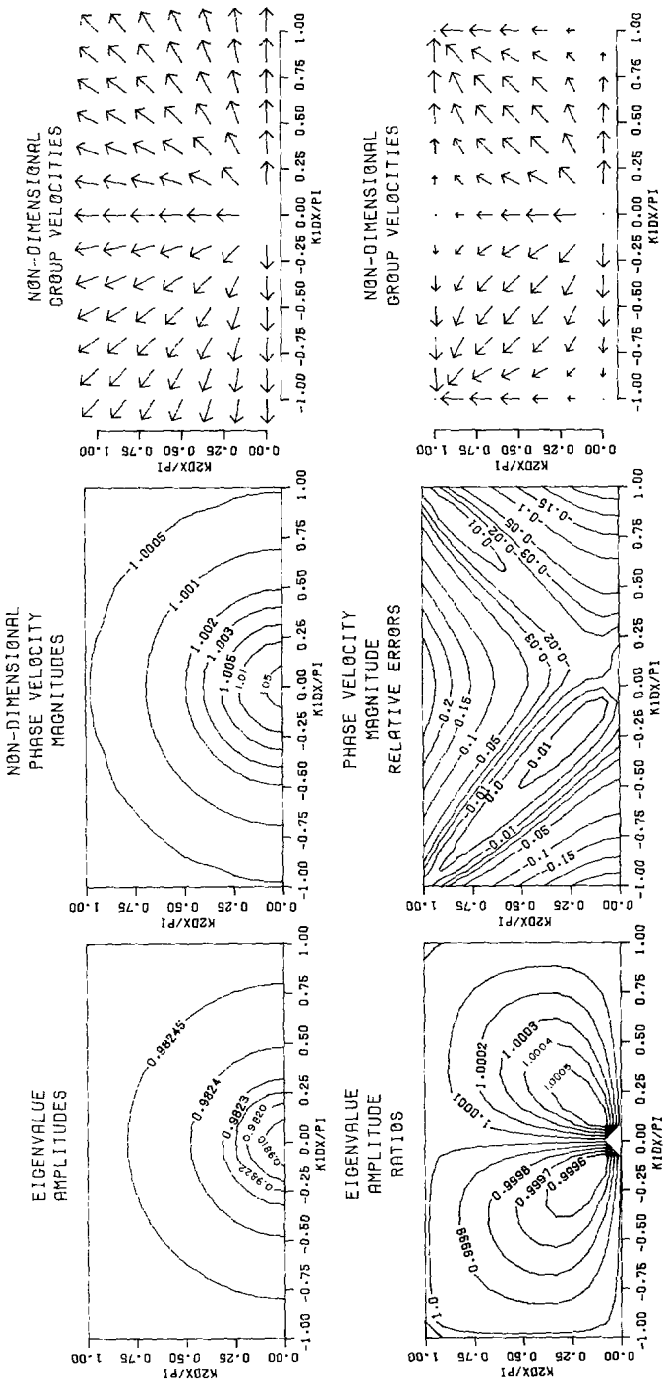

FIG. 3. Analytic solution, RS accuracy measures, and $G/(gh)^{1/2}$ for the parameter values of Fig. 2.

Comparing (10a) with (5a) it is evident that all phase velocity directions are correct. (This may not be true when $\Delta x \neq \Delta y$.) There is, however, some error in $|\mathbf{C}|$. Since the M_C contours are not concentric circles about $(k_1 \Delta x, k_2 \Delta x) = (0, 0)$, the numerical waves are anisotropic. They remain so when $f_3 = 0$.

The RS group velocity vectors are simply gradients of the dispersion surfaces. They display errors in both magnitude and direction. Analytic and RS values have not been shown for the case $(k_1 \Delta x, k_2 \Delta x) = (0, 0)$, which represents infinite sampling per wavelength. Consistency of the numerical solution, however, indicates that for this limit, the RS values approach the analytic. Except for one-dimensional motion (i.e., $k_1 \Delta x = 0$ or $k_2 \Delta x = 0$) directions err toward the diagonal. This suggests that wave energy, which travels at the group velocity, tends to favour this direction. The one-dimensional $2\Delta x$ waves denoted by $(k_1 \Delta x, k_2 \Delta x) = (\pi, 0)$, $(-\pi, 0)$, $(0, \pi)$ are seen to have zero group velocity. This is to be expected since they correspond to saddle points in the dispersion surface. Zero group velocity has also been calculated for the diagonal waves of length $(2)^{1/2} \Delta x$ which are associated with $(k_1 \Delta x, k_2 \Delta x) = (\pi, \pi)$ or $(-\pi, \pi)$. When $\tau = 0$, calculations based on the dispersion relationship in [7] show this to occur when $f_2 < (2)^{-1/2}$.

3. The Galerkin FEM with Piecewise Linear Basis Functions

Within the last decade, FEMs have become popular for solving the shallow water equations. Many such methods are available since typically each combines a spatial discretization with a time stepping or spectral method. Initially, a widely used spatial discretization combined the Galerkin method with piecewise linear basis functions. However, its popularity faded as several authors (e.g., [26, 5]) encountered difficulties with $2\Delta x$ waves. Many authors (e.g., [24]) have studied the source of this problem.

This section examines the accuracy of the Galerkin FEM with piecewise linear basis functions (GLFEM) for two simple triangular elements. As might be expected, the particular shape and configuration of the triangles affect the accuracy of a FEM implementation. Platzman [16] examines two triangular meshes in his study of FEM tidal models, while Mullen and Belytschko [13] study the effects of four meshes on spatial discretizations of the wave equation. Both investigations assume linear basis functions.

The two configurations studied here are meant to be illustrative rather than comprehensive. They are shown in Fig. 4. Both contain six equal triangles with the three variables z, u, and v defined at each vertex or node. The first mesh involves right triangles. A mirror image of the particular case $\Delta x = \Delta y$ is examined in [13].

The second mesh contains isosceles triangles and is considered in [16]. The special case of equilateral triangles is studied in [13]. Because of its symmetry, one would intuitively expect equilateral triangles to be more accurate. Indeed, Mullen and Belytschko conclude that for their problem, this arrangement almost removes the directional dependence of phase velocity. Numerical experiments [8] have also demonstrated that equilateral triangles are more accurate than right triangles.

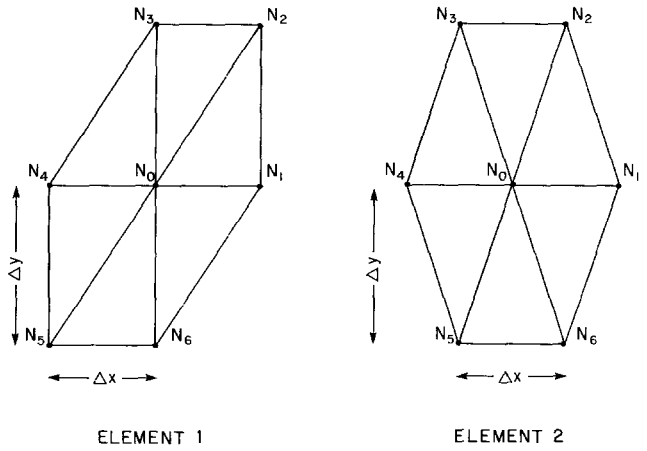

FIG. 4. Triangular element configurations for the FEM analyses.

Imposing the Galerkin condition with the basis function corresponding to node N_0 in element 1, the spatially discretized versions of (1) become

$$\frac{\partial}{\partial t}\left[\frac{1}{2}z_0+\frac{1}{12}(z_1+z_2+z_3+z_4+z_5+z_6)\right]$$
$$+h\left[\frac{2}{3}\left(\frac{u_1-u_4}{2\Delta x}\right)+\frac{1}{6}\left(\frac{u_2-u_3}{\Delta x}\right)+\frac{1}{6}\left(\frac{u_6-u_5}{\Delta x}\right)\right]$$
$$+h\left[\frac{2}{3}\left(\frac{v_3-v_6}{2\Delta y}\right)+\frac{1}{6}\left(\frac{v_2-v_1}{\Delta y}\right)+\frac{1}{6}\left(\frac{v_4-v_5}{\Delta y}\right)\right]=0 \tag{12a}$$

$$\left(\frac{\partial}{\partial t}+\tau\right)\left[\frac{1}{2}u_0+\frac{1}{12}(u_1+u_2+u_3+u_4+u_5+u_6)\right]$$
$$+g\left[\frac{2}{3}\left(\frac{z_1-z_4}{2\Delta x}\right)+\frac{1}{6}\left(\frac{z_2-z_3}{\Delta x}\right)+\frac{1}{6}\left(\frac{z_6-z_5}{\Delta x}\right)\right]$$
$$-f\left[\frac{1}{2}v_0+\frac{1}{12}(v_1+v_2+v_3+v_4+v_5+v_6)\right]=0 \tag{12b}$$

$$\left(\frac{\partial}{\partial t}+\tau\right)\left[\frac{1}{2}v_0+\frac{1}{12}(v_1+v_2+v_3+v_4+v_5+v_6)\right]$$
$$+g\left[\frac{2}{3}\left(\frac{z_3-z_6}{2\Delta y}\right)+\frac{1}{6}\left(\frac{z_2-z_1}{\Delta y}\right)+\frac{1}{6}\left(\frac{z_4-z_5}{\Delta y}\right)\right]$$
$$+f\left[\frac{1}{2}u_0+\frac{1}{12}(u_1+u_2+u_3+u_4+u_5+u_6)\right]=0. \tag{12c}$$

The algebra required to derive these ordinary differential equations (ODEs) is facilitated by the "triangular area coordinates" described by Pinder and Gray [14].

The analogous result for element 2 is

$$\frac{\partial}{\partial t}\left[\frac{1}{2}z_0+\frac{1}{12}(z_1+z_2+z_3+z_4+z_5+z_6)\right]$$
$$+h\left[\frac{2}{3}\left(\frac{u_1-u_4}{2\Delta x}\right)+\frac{1}{6}\left(\frac{u_2-u_3}{\Delta x}\right)+\frac{1}{6}\left(\frac{u_6-u_5}{\Delta x}\right)\right]$$
$$+h\left[\frac{1}{2}\left(\frac{v_2-v_6}{2\Delta y}\right)+\frac{1}{2}\left(\frac{v_3-v_5}{2\Delta y}\right)\right]=0 \tag{13a}$$

$$\left(\frac{\partial}{\partial t}+\tau\right)\left[\frac{1}{2}u_0+\frac{1}{12}(u_1+u_2+u_3+u_4+u_5+u_6)\right]$$
$$+g\left[\frac{2}{3}\left(\frac{z_1-z_4}{2\Delta x}\right)+\frac{1}{6}\left(\frac{z_2-z_3}{\Delta x}\right)+\frac{1}{6}\left(\frac{z_6-z_5}{\Delta x}\right)\right]$$
$$-f\left[\frac{1}{2}v_0+\frac{1}{12}(v_1+v_2+v_3+v_4+v_5+v_6)\right]=0 \tag{13b}$$

$$\left(\frac{\partial}{\partial t}+\tau\right)\left[\frac{1}{2}v_0+\frac{1}{12}(v_1+v_2+v_3+v_4+v_5+v_6)\right]$$
$$+g\left[\frac{1}{2}\left(\frac{z_2-z_6}{2\Delta y}\right)+\frac{1}{2}\left(\frac{z_3-z_5}{2\Delta y}\right)\right]$$
$$+f\left[\frac{1}{2}u_0+\frac{1}{12}(u_1+u_2+u_3+u_4+u_5+u_6)\right]=0. \tag{13c}$$

Assuming the plane wave solutions

$$\begin{pmatrix} z(r\Delta x, s\Delta y, t)\\ u(r\Delta x, s\Delta y, t)\\ v(r\Delta x, s\Delta y, t)\end{pmatrix}=\begin{pmatrix} z_0\\ u_0\\ v_0\end{pmatrix}\exp[i(rk_1\Delta x+sk_2\Delta y-\omega t)] \tag{14}$$

dispersion relationships due solely to these spatial discretizations can be found. Both are calculated from the cubic polynomials which result when requiring nonzero values for z_0, u_0, and v_0. For element 1, the cubic is

$$\omega^3A^2+2i\omega^2A^2\tau+\omega\left[-A^2(f^2+\tau^2)-gh\left(\frac{G_x^2}{(\Delta x)^2}+\frac{G_y^2}{(\Delta y)^2}\right)\right]$$
$$-i\tau gh\left(\frac{G_x^2}{(\Delta x)^2}+\frac{G_y^2}{(\Delta y)^2}\right)=0 \tag{15}$$

where

$$A = \tfrac{1}{2} + \tfrac{1}{6}[\cos k_1 \Delta x + \cos k_2 \Delta y + \cos(k_1 \Delta x + k_2 \Delta y)] \tag{16a}$$

$$G_x = \tfrac{2}{3} \sin k_1 \Delta x - \tfrac{1}{3} \sin k_2 \Delta y + \tfrac{1}{3} \sin(k_1 \Delta x + k_2 \Delta y) \tag{16b}$$

$$G_y = \tfrac{2}{3} \sin k_2 \Delta y - \tfrac{1}{3} \sin k_1 \Delta x + \tfrac{1}{3} \sin(k_1 \Delta x + k_2 \Delta y). \tag{16c}$$

Walters and Carey [24] obtain this result for the particular case $f = \tau = 0$ and $\Delta x = \Delta y$. With $f = \tau = 0$ and either k_1 or k_2 equal to zero, the nontrivial dispersion relationships arising from (15) and (16) are the same as those for the one-dimensional analysis in [2].

For element 2, the cubic polynomial is unchanged but

$$A = \tfrac{1}{2} + \tfrac{1}{6} \cos k_1 \Delta x + \tfrac{1}{3} \cos(\tfrac{1}{2} k_1 \Delta x) \cos k_2 \Delta y \tag{17a}$$

$$G_x = \tfrac{2}{3}[\sin k_1 \Delta x + \sin(\tfrac{1}{2} k_1 \Delta x) \cos k_2 \Delta y] \tag{17b}$$

$$G_y = \sin k_2 \Delta y \cos(\tfrac{1}{2} k_1 \Delta x). \tag{17c}$$

Again, with $f = \tau = 0$ and $k_1 = 0$, the nontrivial dispersion relationships simplify to the one-dimensional result. With equilateral triangles, this simplification also occurs when $k_1 = (3)^{1/2} k_2$.

Phase velocities, group velocities, and wave amplitude decay factors can be calculated from the roots of (15). However, their accuracy does not always indicate the accuracy of the fully discretized numerical solution. In some cases, a subsequent time discretization may partially cancel the errors arising from the spatial discretization, thereby making the fully discretized equations more accurate. It is therefore advisable to continue the analysis by introducing a particular time stepping method for solving the system of ODEs given by (12) or (13).

The one-dimensional analysis of [2] suggests that Crank–Nicolson (CN) is the best time stepping method to use in combination with the GLFEM. It approximates the simple ODE

$$\frac{\partial y}{\partial t} = f(y) \tag{18}$$

with the two-step difference equation

$$\frac{y^{n+1} - y^n}{\Delta t} = \frac{1}{2}(f^{n+1} + f^n). \tag{19}$$

Dispersion relationships are calculated for the fully discretized equations by assuming the plane wave solutions

$$\begin{pmatrix} z(r \Delta x, s \Delta y, n \Delta t) \\ u(r \Delta x, s \Delta y, n \Delta t) \\ v(r \Delta x, s \Delta y, n \Delta t) \end{pmatrix} = \begin{pmatrix} z_0 \\ u_0 \\ v_0 \end{pmatrix} \exp[i(r k_1 \Delta x + s k_2 \Delta y - n \omega \Delta t)]. \tag{20}$$

In particular, the numerical eigenvalues defined by (8b) are calculated as

$$\lambda = (1 - \tfrac{1}{2}i\omega_0 \Delta t)/(1 + \tfrac{1}{2}i\omega_0 \Delta t) \tag{21}$$

where ω_0 is a root of (15). This is seen by comparing the dispersion relationships for (18) and (19).

In order to compare the relative accuracy of elements 1 and 2 in Fig. 4, the total area of the elements should be considered. Since both elements have the same storage requirements for the nodal variables, equal area implies equal storage costs for a model of prespecified spatial dimensions. Accuracy can then be compared on an equal-cost basis. In particular, consider $\Delta x = \Delta y$ in element 1, and equilateral triangles with sides of length d in element 2. Equal area then requires

$$d = (\tfrac{4}{3})^{1/4} \Delta x. \tag{22}$$

In order that the accuracy of these two FEMs might also be compared to the RS results, the parameters of (9) should be redefined for triangular elements. Specifically

$$f_1 = \tau \left(\frac{2A_\Gamma}{gh}\right)^{1/2} \tag{23a}$$

$$f_2 = \left(\frac{gh}{2A_\Gamma}\right)^{1/2} \Delta t \tag{23b}$$

$$f_3 = f \left(\frac{2A_\Gamma}{gh}\right)^{1/2} \tag{23c}$$

where A_Γ is the area of each triangle in the respective element. With $\Delta x = \Delta y$ in element 1, (23) and (9) become equal. Moreover, per unit area, RS has as many variables as the FEMs.

With equilateral triangles, it is convenient to redefine G_y in (17). Setting

$$G_y = [2 \sin k_2 \Delta y \cos(\tfrac{1}{2}k_1 \Delta x)]/3^{1/2} \tag{24}$$

with $\Delta x = d$ and $\Delta y = (3)^{1/2} d/2$ permits the replacement of $G_y/\Delta y$ with G_y/d in (15).

Figure 5 shows dispersion surfaces for the same parameter values as in Fig. 2. It also has the same scale and is viewed from the same perspective. Surfaces are shown for both elements of Fig. 4 and both the spatially discretized and fully discretized equations. Again, only positive $k_2 \Delta x$ need be displayed since (15) is symmetric through the origin for element 1, and both through the origin and about the $k_2 d$ axis for element 2.

Figure 5 has several notable points. The first is that there is little difference between the spatially discretized and fully discretized surfaces. This implies that virtually all the inaccuracy of the fully discretized equations is due to the spatial discretization. Hence CN has scarcely affected the accuracy. This may not be true for all time stepping schemes.

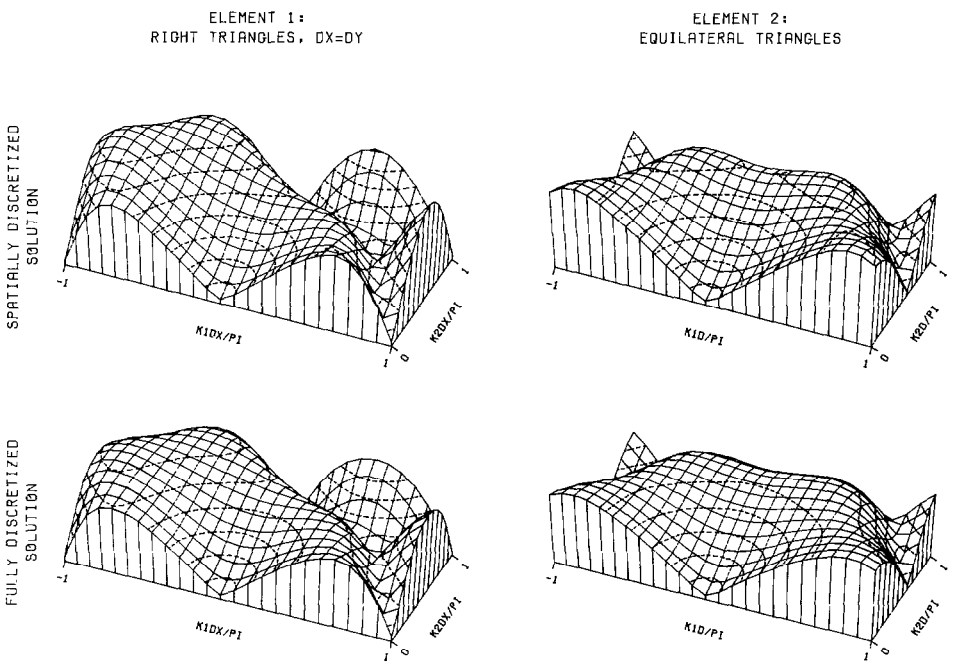

FIG. 5. Dispersion surfaces ($|\omega|\Delta x/(\pi(gh)^{1/2})$) for the GLFEM with CN time stepping. Parameter values are $f_1 = 0.05, f_2 = 0.7071, f_3 = 0.10$. Dotted line contours are in increments of 0.10.

Each of the dispersion surfaces in Fig. 5 is symmetric. Considering the symmetries in the elements themselves, these are to be expected. The surface for element 1 is symmetric about the planes $k_2 = k_1$ and $k_2 = -k_1$. The element 2 surface is symmetric about $k_2 = (\tan\phi)\, k_1$, where $\phi = 30°$, 60°, 90°, 120°, or 150°.

The most striking feature of both surfaces is their poor accuracy for higher values of wavenumber sampling. Accuracy is reasonable for small wavenumbers (i.e., $k\,\Delta x/\pi < 0.1$) but it deteriorates as $k\,\Delta x$ increases. This is consistent with the one-dimensional analysis [2]. Particularly disturbing are the frequency valleys. For the case $\tau = 0$, the nontrivial roots of (15) are

$$\omega = \pm \left[f^2 + \frac{gh}{A^2} \left(\frac{G_x^2}{(\Delta x)^2} + \frac{G_y^2}{(\Delta y)^2} \right) \right]^{1/2}. \tag{25}$$

Assuming $\Delta x = \Delta y$, minimal values of $|\omega|$ occur when

$$G_x^2 = G_y^2 = 0. \tag{26}$$

In particular, for element 1 they occur at the following seven values of $(k_1\,\Delta x/\pi, k_2\,\Delta x/\pi)$: (0, 0), (1, 1), (−1, 1), (0, 1), (1, 0), (−1, 0), $(\frac{2}{3}, \frac{2}{3})$. The latter corresponds to a diagonal wave of length $(4.5)^{1/2}\,\Delta x$, while the fourth, fifth, and sixth minimal values are associated with one-dimensional $2\,\Delta x$ waves. The second and third minima

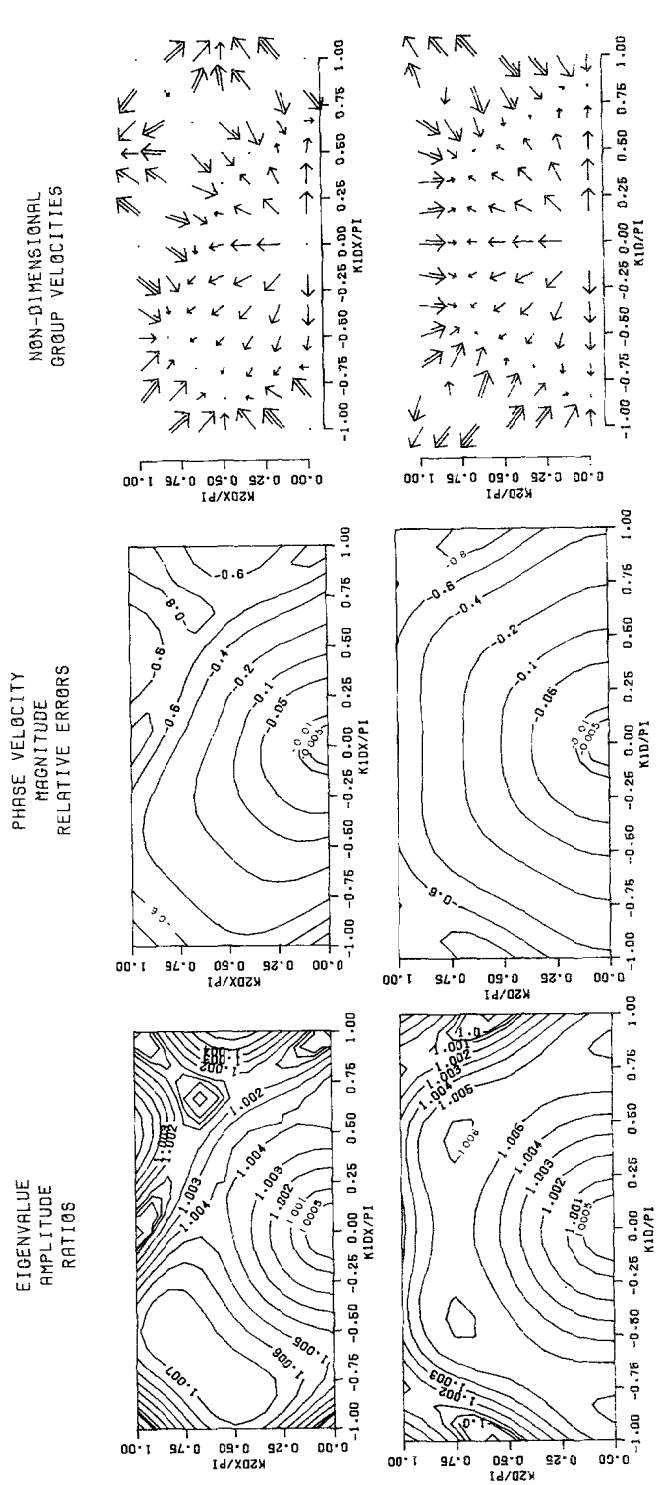

FIG. 6. M_A, M_C, and $\mathbf{G}/(gh)^{1/2}$ for the GLFEM with CN time stepping and the parameter values of Fig. 5. Each full shaft of multi-shafted vectors denotes 1 unit (i.e., $|\mathbf{G}| = (gh)^{1/2}$).

581/56/2-9

correspond to diagonal waves of length $(2)^{1/2}\,\Delta x$. (In a two-dimensional grid, plane waves shorter than $2\,\Delta x$ are possible.) All these waves have the inertial frequency f. In the particular case when $f=0$, $\omega=|\mathbf{C}|=0$ at these seven points. Hence the progressive and retrogressive surfaces touch. These seven minimal values for $|\omega|$ are perturbed slightly by the nonzero values of τ in Fig. 5.

For element 2, the surface minima occur at the $(k_1 d/\pi, k_2 d/\pi)$ values $(0,0)$, $(1,(3)^{-1/2})$, and $(-1,(3)^{-1/2})$. The latter two correspond to waves of length $(3)^{1/2}\,d$. A similar minimum also exists at $(0,2(3)^{-1/2})$ but is not shown.

Comparing accuracy on the basis of equal area now means that $k_1\,\Delta x \neq k_1\,d$. That is, even though waves may have the same lengths on the element 1 and element 2 meshes, their sampling rates per wavelength will differ. The shortest one-dimensional wave supported by element 1 is $2\,\Delta x$ while for element 2 it is the slightly longer value of $2d$. In order to permit accuracy comparisons on the basis of wavelength, the $k_1 d$ and $k_2 d$ axes should be scaled. This is done in Fig. 6.

Figure 6 shows M_A, M_C, and $\mathbf{G}/(gh)^{1/2}$ values associated with the fully discretized dispersion surfaces of Fig. 5. Both element configurations produce wave amplitudes which are too large and phase velocities which are too small. However, for both M_A and M_C, when $k_1\,\Delta x/\pi < 0.5$ the element 2 contour levels are further away from $(k_1, k_2)=(0,0)$ than those of element 1. This implies that element 2 is more accurate for longer waves.

Comparing Fig. 6 with Fig. 3, one cannot conclude that either numerical scheme is consistently more accurate. Generally the RS scheme is more accurate, however, there are some regions near $(k_1\,\Delta x, k_2\,\Delta x)=(0,0)$ where the GLFEM schemes are better for both wave amplitude and phase velocity.

The accuracy of the GLFEM numerical group velocity deteriorates significantly as the wavenumber increases. Errors exist in both magnitude and direction. In fact, for some short waves, $\mathbf{G}$ is not only much too large but also in virtually the opposite direction that it should be. Group and phase velocities which are not co-directional signify energy propagating in a different direction than the wave crests. Although this should not occur for shallow water waves, it is clearly seen to do so for both the RS and GLFEM schemes.

4. Thacker's Irregular Grid Finite Difference Technique

Thacker [20–22] has recently presented a technique for defining FDMs over irregular grids composed of triangular elements. The underlying concept is that in the vicinity of a triangle, the partial derivatives of a function can be approximated by the slopes of a plane determined by the values of the function at the vertices. At a vertex, the partial derivatives are then approximated by a weighted average of the approximations in each of the triangles which contain that vertex. For equal area triangles such as those of Fig. 4, the resultant spatial derivative approximations are equivalent to those for the GLFEM. In fact, for elements 1 and 2, respectively, the spatially

discretized equations are simply found by replacing all terms of the form $1/2z_0 + \frac{1}{12}(z_1 + z_2 + z_3 + z_4 + z_5 + z_6)$ in (12) and (13) with z_0. When combined with an explicit time stepping scheme, Wang [25] points out that the fully discretized technique is a "lumped mass matrix" version of the GLFEM.

Thacker employs an explicit leapfrog time stepping similar to the RS scheme of Section 2. For solving (1), his fully discretized equations may be generalized as

$$\frac{z_j^{n+1} - z_j^n}{\Delta t} + h\left(\widehat{\frac{\partial u}{\partial x}}\right)_j^{n+1/2} + h\left(\widehat{\frac{\partial v}{\partial y}}\right)_j^{n+1/2} = 0 \tag{27a}$$

$$\frac{u_j^{n+1/2} - u_j^{n-1/2}}{\Delta t} + g\left(\widehat{\frac{\partial z}{\partial x}}\right)_j^{n} - f[\theta v_j^{n+1/2} + (1-\theta)\, v_j^{n-1/2}] + \tau[\theta u_j^{n+1/2} + (1-\theta)\, u_j^{n-1/2}] = 0 \tag{27b}$$

$$\frac{v_j^{n+1/2} - v_j^{n-1/2}}{\Delta t} + g\left(\widehat{\frac{\partial z}{\partial y}}\right)_j^{n} + f[\theta u_j^{n+1/2} + (1-\theta)\, u_j^{n-1/2}] + \tau[\theta v_j^{n+1/2} + (1-\theta)\, v_j^{n-1/2}] = 0 \tag{27c}$$

where

$$\left(\widehat{\frac{\partial}{\partial x}}\right) \quad \text{and} \quad \left(\widehat{\frac{\partial}{\partial y}}\right)$$

denote the spatial derivative approximations. For elements 1 and 2, these approximations are identical to those in (12) and (13). The particular scheme discussed by Thacker has $\tau = 0$ and $\theta = 1$.

Assuming a uniform grid of equilateral triangles and $f = 0$, Thacker [22] calculates dispersion relationships for his scheme. These results can be extended to include the element 1 grid with $\Delta x = \Delta y$, and to allow for nonzero friction and Coriolis parameters. For both grids, the spatially discretized relationships are simply found by setting $A = 1$ in (15).

Assuming plane wave solutions, the characteristic equation arising from (27) is

$$(\lambda - 1)\{[\lambda(1 + \theta\tau\,\Delta t) - 1 + (1-\theta)\,\tau\,\Delta t]^2 + (f\,\Delta t)^2(\lambda\theta + (1-\theta))^2\} + gh(\Delta t)^2\,\lambda[\lambda(1 + \theta\tau\,\Delta t) - 1 + (1-\theta)\,\tau\,\Delta t]\left(\frac{G_x^2}{(\Delta x)^2} + \frac{G_y^2}{(\Delta y)^2}\right) = 0 \tag{28}$$

with λ defined as in (8b) and G_x, G_y as in (16), or (17) and (24). With $\tau = 0$, the respective dispersion relationships for elements 1 and 2 are

$$\cos\omega\,\Delta t = \left[1 - (f\,\Delta t)^2\,\theta(1-\theta) - \frac{1}{2}gh\left(\frac{\Delta t}{\Delta x}\right)^2 G_{xy}\right] \Big/ (1 + (\theta f\,\Delta t)^2) \tag{29a}$$

and

$$\cos \omega \Delta t = \left[1 - (f\Delta t)^2 \theta(1-\theta) - \frac{1}{2} gh \left(\frac{\Delta t}{d}\right)^2 G_{xy}\right] \Big/ (1 + (\theta f \Delta t)^2) \tag{29b}$$

where

$$G_{xy} = G_x^2 + G_y^2. \tag{29c}$$

With $f = 0$, (29b) simplifies to Thacker's result.

For equilateral triangles, Thacker obtains the following necessary stability conditions for his scheme and the GLFEM with similar time stepping:

$$f_2' = (gh)^{1/2} \Delta t/d \leqslant 1.70437 \tag{30a}$$

$$f_2' \leqslant 0.90288. \tag{30b}$$

These conditions assume $f = 0$ and $\theta = 1$. For element 1 with $\Delta x = \Delta y$, the analogous conditions are

$$f_2 = (gh)^{1/2} \Delta t/\Delta x \leqslant 1.4142 \tag{31a}$$

$$f_2 \leqslant 0.79830. \tag{31b}$$

On the basis of equal area, element 2 has less restrictive stability constraints than element 1. Furthermore, for both grids Thacker's scheme is less restrictive than its GLFEM counterpart. This means that Thacker's scheme can use a larger time step. Increased stability with lumping is also noted by Strang and Fix [19].

Thacker claims that his scheme is most accurate with the maximum possible time step. This can be verified with an asymptotic analysis. Assume $\tau = 0$, f_2' is $O(1)$, and f_3 and kd are small. Comparing terms in the asymptotic expansion of (29b) and the corresponding analytic expansion of $\cos(\omega \Delta t)$ shows that

$$f_2' = (3)^{1/2} \tag{32}$$

and

$$\theta = \tfrac{1}{2}$$

produce the best match. Accuracy is also seen to increase as f_2' approaches $(3)^{1/2}$ from below. Notice that the optimal value of f_2' is slightly larger than the stability limit given in (30a).

For right triangles with $\Delta x = \Delta y$, a similar analysis is less conclusive. Accuracy of

the numerical method is now dependent on wave direction as well as f_2. In particular, the most accurate value of f_2 for wave propagation is

$$f_2 = 2\left(1 + \frac{xy}{x^2 + y^2}\right)^{1/2} \tag{33}$$

where $x = k_1 \Delta x$ and $y = k_2 \Delta x$. The minimal optimal value is $(2)^{1/2}$ when $x = -y$. As seen from (31a) this is also the maximum stable value. $\theta = \frac{1}{2}$ still provides the most accurate representation of the Coriolis terms.

Figure 7 shows the dispersion surfaces for the spatially and fully discretized versions of Thacker's scheme. It has the same parameter values, scale, and perspective as Fig. 2 and Fig. 5. The spatially discretized surfaces are simply lumped versions of those in Fig. 5. They have the same characteristic shape but, as seen from the dotted line contour levels, have smaller values. Again, the time stepping method has little effect on the fully discretized surface values. The symmetries and location of the surface minima are the same for Fig. 7 as for Fig. 5. This implies that problems with short waves for the GLFEM can also be expected with Thacker's scheme.

Figure 8 displays the two accuracy measure functions and group velocity vectors corresponding to the surfaces of Fig. 7. As with the GLFEM, the element 2 mesh is generally more accurate than the element 1. Figure 9 is similar but has the near optimal parameter values $\theta = \frac{1}{2}$, and $f_2 = 1.40$, $f_2 = 1.826$ $(f_2' = 1.70)$ for the right triangle and equilateral triangle cases, respectively. As theory predicts, Fig. 9 does

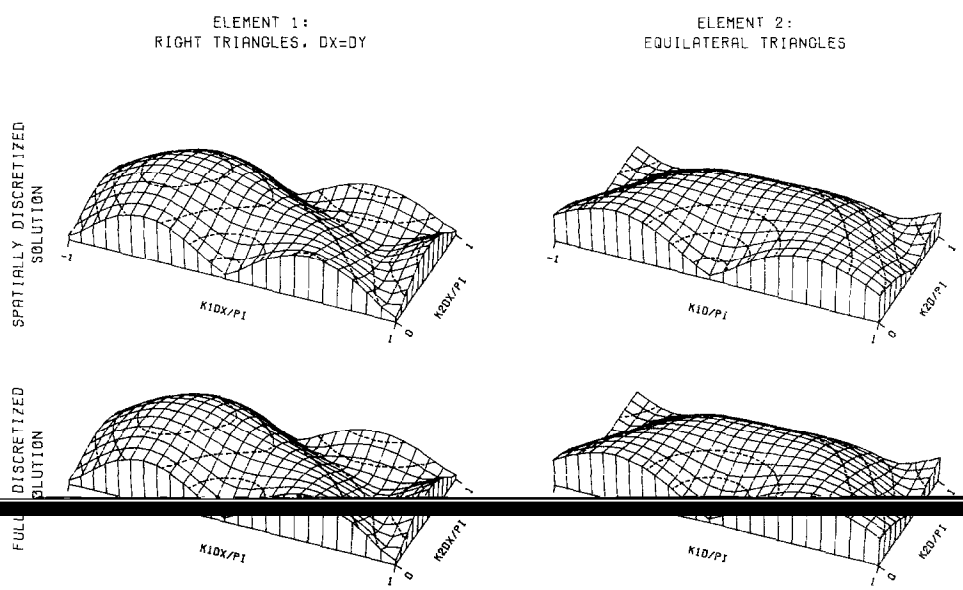

FIG. 7. Dispersion surfaces $(|\omega| \Delta x/(\pi(gh)^{1/2}))$ for Thacker's method. Parameter values are $f_1 = 0.05$, $f_2 = 0.7071$, $f_3 = 0.10$, $\theta = 1$. Dotted line contours are in increments of 0.10.

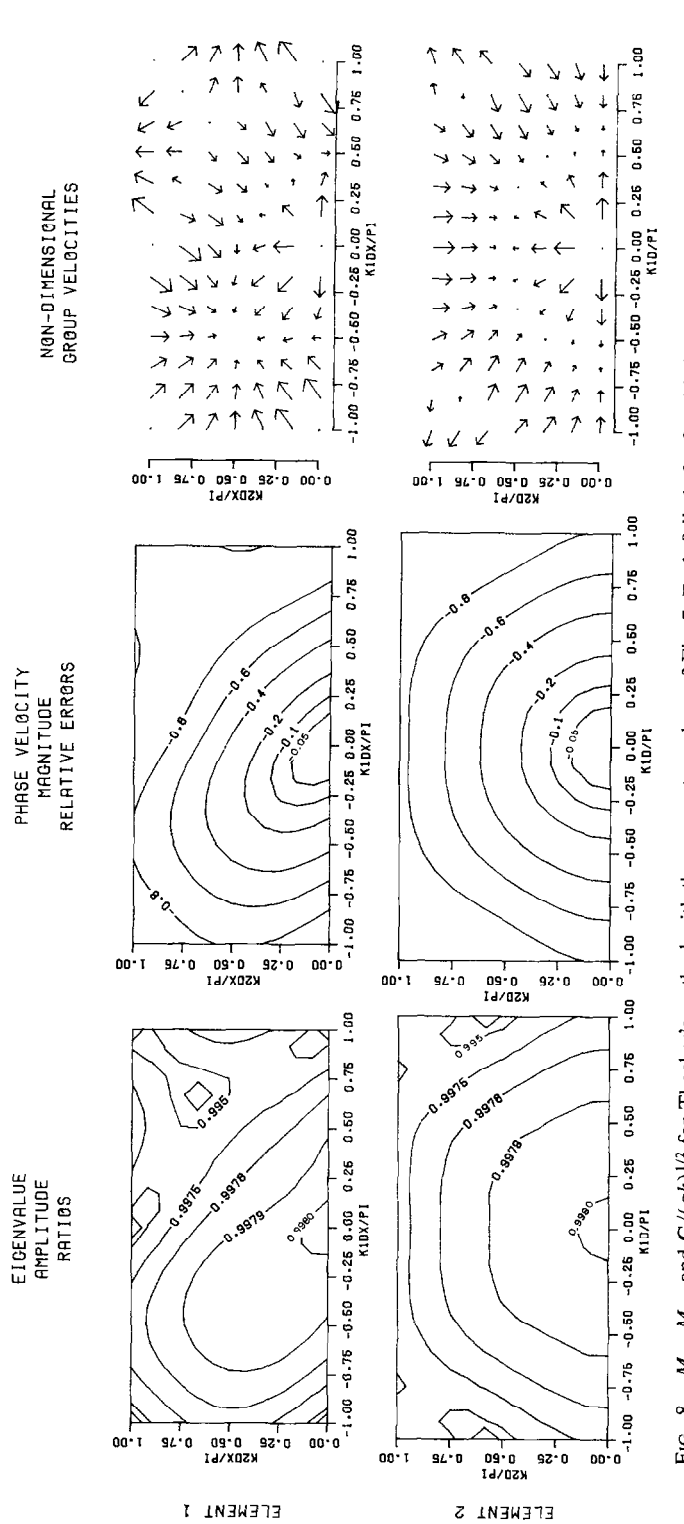

FIG. 8. M_A, M_C, and $G/(gh)^{1/2}$ for Thacker's method with the parameter values of Fig. 7. Each full shaft of multi-shafted vectors denotes 1 unit (i.e., $|\mathbf{G}| = (gh)^{1/2}$).

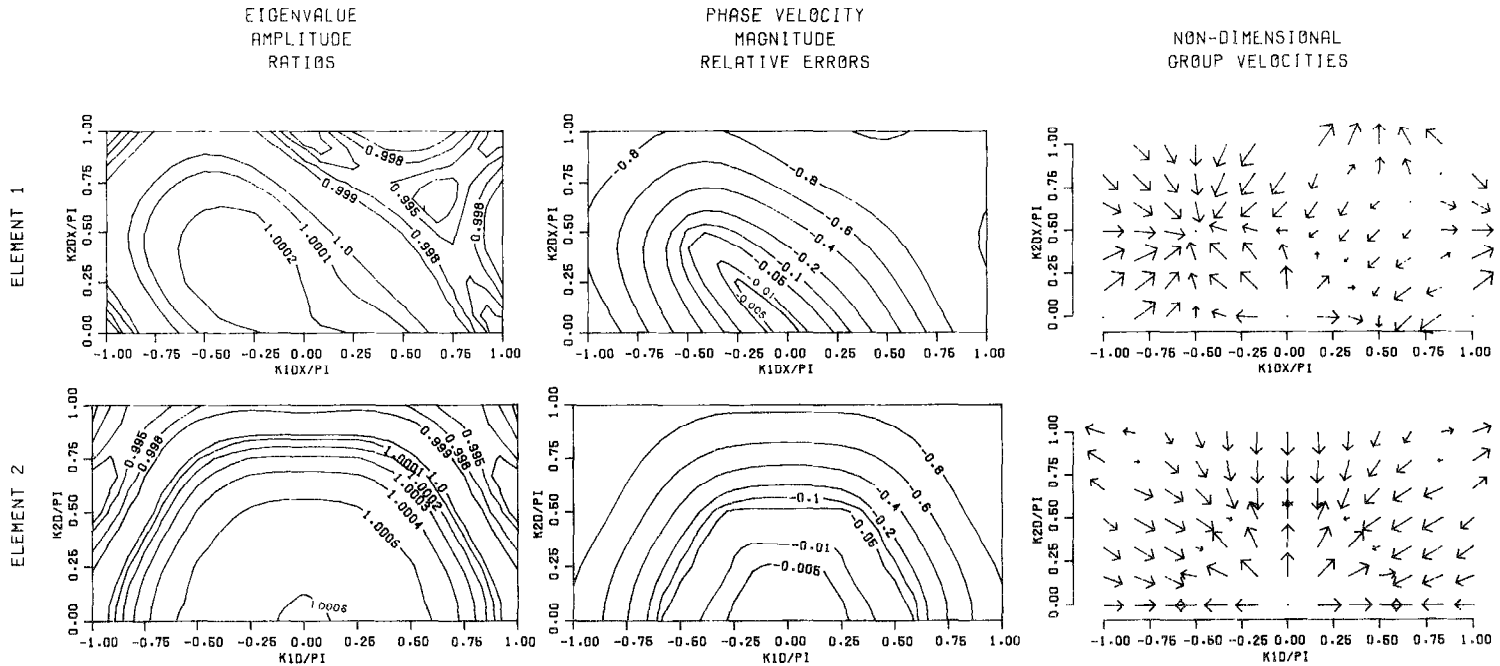

FIG. 9. M_A, M_C, and $\mathbf{G}/(gh)^{1/2}$ for Thacker's method with $f_1 = 0.05, f_3 = 0.10$, and $\theta = 0.5$. $f_2 = 1.40$ for element 1 and $f_2' = 1.70$ for element 2. Each full shaft of multi-shafted vectors denotes 1 unit (i.e., $|\mathbf{G}| = (gh)^{1/2}$).

display more accurate $|\mathbf{C}|$ and $\mathbf{G}$ for small wavenumbers. The amplitude ratios are also more accurate, though they are too large in Fig. 9 and too small in Fig. 8. Notice that for small increasing wavenumbers, Fig. 9 shows an improvement in amplitude accuracy.

A comparison of Fig. 8 and Fig. 6 demonstrates that mass lumping can cause an accuracy loss. However, to some extent, the different time stepping methods for the two techniques has influenced the accuracy measure values. Replacing the CN time stepping used with the GLFEM of Fig. 6 with Thacker's time stepping actually improves, for the same parameter values, the element 2 accuracy. However, Thacker's scheme remains less accurate for both elements.

A comparison of Fig. 9 with Fig. 6 is also revealing. It illustrates that an optimal Thacker scheme can be more accurate than the unlumped FEM to which it is related. Considering the much smaller costs of running Thacker's scheme, this is a significant result. However, the most accurate Thacker's scheme is not more accurate than the most accurate GLFEM, since the latter improves as f_2 decreases. Nevertheless, Thacker's scheme can be made as accurate as the GLFEM by increasing its spatial resolution. The associated cost increase is more than offset by the explicit time stepping, so that his scheme remains cheaper.

5. The "Wave Equation" Model for Finite Element Tidal Computations

Recently Gray and Lynch [4, 11] introduced a promising FEM for solving the shallow water equations. Rather than working with the governing equations in conservation form, their "wave equation" method (WEM) involves transforming the continuity equation to a second-order partial differential equation (PDE). The revised system of equations is then solved with a Galerkin FEM, piecewise linear basis functions, and centred time stepping. Dispersion analyses of the one-dimensional WEM and its lumped counterpart, the LWEM, are given in [3]. This section extends those results to the two-dimensional triangular elements of Fig. 4.

The linearized, two-dimensional, constant depth version of the continuity equation solved by Lynch and Gray [11] is

$$\frac{\partial^2 z}{\partial t^2} + \tau \frac{\partial z}{\partial t} - gh\left(\frac{\partial^2 z}{\partial x^2} + \frac{\partial^2 z}{\partial y^2}\right) + hf\left(\frac{\partial v}{\partial x} - \frac{\partial u}{\partial y}\right) = 0. \tag{34}$$

It is solved in combination with the momentum equations (1b) and (1c). The characteristic equation for this system of PDEs is simply the product of (4) and $(-i\omega + \tau)$. Consequently, replacing (1a) with (34) produces an additional dispersion relationship whose associated solution is a stationary wave that decays in time when $\tau > 0$.

Since Lynch and Gray employ piecewise linear approximating functions, the Laplacian term in (34) necessitates a weak form of the Galerkin condition. Imposing

this condition with the basis function corresponding to node N_0 in element 1, the spatially discretized version of (34) becomes

$$\left(\frac{\partial}{\partial t^2}+\tau\frac{\partial}{\partial t}\right)\left[\frac{1}{2}z_0+\frac{1}{12}(z_1+z_2+z_3+z_4+z_5+z_6)\right]$$
$$+hf\left[\frac{2}{3}\left(\frac{v_1-v_4}{2\Delta x}\right)+\frac{1}{6}\left(\frac{v_2-v_3}{\Delta x}\right)+\frac{1}{6}\left(\frac{v_6-v_5}{\Delta x}\right)\right]$$
$$-hf\left[\frac{2}{3}\left(\frac{u_3-u_6}{2\Delta y}\right)+\frac{1}{6}\left(\frac{u_2-u_1}{\Delta y}\right)+\frac{1}{6}\left(\frac{u_4-u_5}{\Delta y}\right)\right]$$
$$-gh\left[\frac{z_1-2z_0+z_4}{(\Delta x)^2}+\frac{z_3-2z_0+z_6}{(\Delta y)^2}\right]=0. \tag{35}$$

The analogous result for element 2 is

$$\left(\frac{\partial^2}{\partial t^2}+\tau\frac{\partial}{\partial t}\right)\left[\frac{1}{2}z_0+\frac{1}{12}(z_1+z_2+z_3+z_4+z_5+z_6)\right]$$
$$+hf\left[\frac{2}{3}\left(\frac{v_1-v_4}{2\Delta x}\right)+\frac{1}{6}\left(\frac{v_2-v_3}{\Delta x}\right)+\frac{1}{6}\left(\frac{v_6-v_5}{\Delta x}\right)\right]$$
$$-hf\left[\frac{1}{2}\left(\frac{u_2-u_6}{2\Delta y}\right)+\frac{1}{2}\left(\frac{u_3-u_5}{2\Delta y}\right)\right]$$
$$-gh\left\{\frac{z_1-2z_0+z_4}{(\Delta x)^2}+\frac{1}{(\Delta y)^2}\left[\frac{1}{4}(z_2-z_1-z_0+z_6)\right.\right.$$
$$\left.\left.+\frac{1}{4}(z_3-z_0-z_4+z_5)+\frac{1}{2}\left[\frac{1}{2}(z_2+z_3+z_6+z_5)-2z_0\right]\right]\right\}=0. \tag{36}$$

The associated spatially discretized momentum equations are given by (12b), (12c) and (13b), (13c), respectively.

Assuming plane wave solutions of the form (14), dispersion relationships can be found for these spatial discretizations. In both cases they are derived from the roots of the polynomial

$$\omega^4+3i\tau\omega^3-\omega^2(3\tau^2+f^2+2ghB/A)-i\tau\omega(\tau^2+f^2+4ghB/A)$$
$$+gh\left[2(\tau^2+f^2)B/A-f^2\left(\frac{G_y^2}{(\Delta y)^2}+\frac{G_x^2}{(\Delta x)^2}\right)\Big/A^2\right]=0. \tag{37}$$

For element 1, A, G_x, and G_y are defined by (16) while

$$B=\frac{1-\cos k_1\Delta x}{(\Delta x)^2}+\frac{1-\cos k_2\Delta y}{(\Delta y)^2}. \tag{38a}$$

For element 2, A, G_x, and G_y are defined by (17) while

$$B = \frac{1 - \cos k_1 \Delta x}{(\Delta x)^2} + \frac{\frac{1}{4}(3 + \cos k_1 \Delta x) - \cos(\frac{1}{2}k_1 \Delta x) \cos k_2 \Delta y}{(\Delta y)^2}. \tag{38b}$$

Assuming plane wave solutions of the form (20), dispersion relationships can also be calculated for the fully discretized "wave equations." As in [11], we assume that the time stepping method is parameterized in terms of θ, the weighting parameter for the gravity terms, and α, the weighting parameter for the friction terms in the momentum equations. With G_x, G_y, A, and B defined appropriately for elements 1 and 2, the characteristic equation is

$$\left[\gamma_1 + \frac{1}{2}\tau \Delta t \gamma_2 + 2gh(\Delta t)^2 \gamma_\theta B/A\right][\gamma_2^2 + 4\tau \Delta t \gamma_2 \gamma_\alpha + 4(\Delta t)^2(\tau^2 \gamma_\alpha^2 + f^2\lambda^2)]$$

$$- 4gh\lambda^2 f^2 \gamma_\theta (\Delta t)^4 \left(\frac{G_x^2}{(\Delta x)^2} + \frac{G_y^2}{(\Delta y)^2}\right)\Big/A^2 = 0 \tag{39a}$$

where λ is defined in (8b) and

$$\gamma_1 = (\lambda - 1)^2 \tag{39b}$$

$$\gamma_2 = \lambda^2 - 1 \tag{39c}$$

$$\gamma_\theta = \tfrac{1}{2}\theta(\lambda^2 + 1) + (1 - \theta)\lambda \tag{39d}$$

$$\gamma_\alpha = \tfrac{1}{2}\alpha(\lambda^2 + 1) + (1 - \alpha)\lambda. \tag{39e}$$

Two roots of (39) are associated with gravity waves. They are called principal roots. The remaining four roots are either artifacts of the numerical solution, called spurious roots, or approximations to the two stationary modes. Spurious roots are important only insofar as they can contaminate the principal numerical solution. In particular when their magnitude is larger than that of the principal roots, they decay more slowly (or grow more rapidly) and eventually dominate the solution. Provided they do not contaminate the gravity wave solutions, the stationary mode approximations are also unimportant. However, if either f or h were nonconstant, one stationary mode would become a planetary wave whose numerical approximation would be of interest.

A linear stability analysis of the WEM is difficult when f is nonzero. However, necessary stability conditions with realistic nonzero values of f should only be perturbations of the conditions derived by assuming $f = 0$. Therefore, the restrictions obtained by assuming $f = 0$ should be close to those required for nonzero Coriolis. Numerical computations confirm this.

When $f = 0$, (39) reduces to

$$Q_1 Q_2^2 = 0 \tag{40a}$$

where

$$Q_1 = \gamma_1 + \tfrac{1}{2}\tau\,\Delta t\,\gamma_2 + 2gh(\Delta t)^2\,\gamma_\theta B/A \tag{40b}$$

and

$$Q_2 = \gamma_2 + 2\tau\,\Delta t\,\gamma_\alpha . \tag{40c}$$

This result is similar to the one-dimensional characteristic equation [3] $Q_1 Q_2$. Specifically, Q_2 is identical, and Q_1 has the same form when E^2 is defined as

$$E^2 = 2gh(\Delta t)^2 B/A. \tag{41}$$

This similarity implies that the one-dimensional stability analysis can be followed here.

The roots of Q_2 are parasitic. In one dimension, they are stable when [11]

$$\alpha \geqslant \tfrac{1}{2}. \tag{42}$$

In two dimensions, each of the parasitic roots has multiplicity 2, thereby requiring the more restrictive condition $\alpha > \frac{1}{2}$. Numerical computations suggest that $\alpha = 1$ is a good choice since it generally ensures that the spurious root magnitudes are less than those of the principal roots. This is discussed further in [3].

The propagating principal roots of Q_1 are stable when

$$\theta \geqslant -\left(\frac{2}{E^2}\right)\left(1 + \frac{1}{2}\tau\,\Delta t\right) \tag{43a}$$

for all E^2 and $\tau\,\Delta t$. The nonpropagating principal roots are stable when

$$\theta \geqslant \frac{1}{2}\left(1 - \frac{4}{E^2}\right) \tag{43b}$$

for all E^2. Assuming positive $\tau\,\Delta t$, the second condition is more restrictive. For element 1 with $\Delta x = \Delta y$, it reduces to

$$\theta \geqslant \frac{1}{2}\left(1 - \frac{1}{6.4641 f_2^2}\right) \tag{44a}$$

while for the equilateral triangles of element 2 it becomes

$$\theta \geqslant \frac{1}{2}\left(1 - \frac{1}{5.5783(f_2')^2}\right). \tag{44b}$$

With $k_1 = 0$, E^2 is identical to its one-dimensional counterpart. Hence all the roots and the stability constraints reduce to those in [3]. Setting $k_1 = 0$ is equivalent to projecting both elements of Fig. 4 onto the y axis. The six nodes coalesce to three nodes which are uniformly separated by Δy.

In [3] it was possible to choose a value of θ which produces the most accurate one-dimensional dispersion relationship for the WEM. This is also possible in two dimensions. Assuming $f = \tau = 0$, the principal numerical eigenvalues are the roots of

$$(\lambda - 1)^2 + 2gh(\Delta t)^2[\tfrac{1}{2}\theta(\lambda^2 + 1) + (1 - \theta)]B/A = 0. \tag{45}$$

With element 1 and $\Delta x = \Delta y$, substitution for λ leads to the dispersion relationship

$$\cos \omega \Delta t = [1 - (1 - \theta)D]/(1 + \theta D) \tag{46a}$$

where

$$D = f_2^2(2 - \cos x - \cos y)/[\tfrac{1}{2} + \tfrac{1}{6}(\cos x + \cos y + \cos(x + y))] \tag{46b}$$

and $x = k_1 \Delta x$, $y = k_2 \Delta x$. Comparing the asymptotic expansion of (46a) for small x and y with the analytic result does not yield one value of θ which is best for all wave directions. In particular, when $y = sx$,

$$\theta = \frac{1}{6} + \frac{1}{3f_2^2} + \frac{1}{6f_2^2}\left[\frac{2s}{1 + s^2} - \frac{1 + s^4}{(1 + s^2)^2}\right] \tag{47}$$

provides the best match. With $s = 0$ or $s = \infty$, (47) reduces to the one-dimensional result [3]

$$\theta = \frac{1}{6}\left(1 + \frac{1}{f_2^2}\right). \tag{48}$$

This value produces the most accurate representation of wave propagation along either axis of element 1 in Fig. 4. However, for waves propagating along the diagonal (i.e., $s = 1$),

$$\theta = \frac{1}{6} + \frac{5}{12f_2^2} \tag{49}$$

is best. With $f_2 = (2)^{-1/2}$, these two optimal values are appreciably different, namely, $\frac{1}{2}$ and 1.

Accuracy which varies with wave direction is clearly undesirable. It implies that grid orientation affects model accuracy and that by simply changing direction a wave may be less accurately represented. Fortunately, with the preceding simplifying assumptions, this directional dependence can be avoided with equilateral traingles. In fact, it is even avoided for small nonzero values of $\tau \Delta t$.

With $x = k_1 d$, $y = k_2 d$ and $rd = \Delta y$, the dispersion relationship for element 2 is again given by (46a), but

$$D = \frac{(f_2')^2[1 - \cos x + (1/r^2)(\frac{3}{4} + \frac{1}{4}\cos x - \cos(\frac{1}{2}x)\cos(ry))]}{[\frac{1}{2} + \frac{1}{6}\cos x + \frac{1}{3}\cos(\frac{1}{2}x)\cos(ry)]}. \tag{50}$$

Matching asymptotic expansions now shows that

$$\theta = \frac{1}{6} + \frac{1}{8(f_2')^2} \tag{51}$$

is the most accurate value for gravity wave propagation in equilateral triangles. Unlike (47), it is not directionally dependent. Furthermore, with the substitution $\Delta y = ((3)^{1/2}/2)d$, (51) is identical to the one-dimensional result (48).

Figure 10 shows the principal dispersion surfaces for the spatially and fully discretized versions of the WEM. It has the same parameter values, scale, and perspective as Figs. 2, 5, and 7. The time stepping parameters for the fully discretized equations are $\theta = 0.5$ for element 1 and $\theta = 0.45534$ for element 2. The former is optimal for one-dimensional wave propagation along the x or y axis, while the later is optimal for all directions. Both values satisfy the principal eigenvalue stability conditions (44). For both elements, choosing $\alpha = 1$ ensures stability of the parasitic eigenvalues.

Unlike the GLFEM and Thacker's scheme, these surfaces do not have local minima at large wavenumbers. This implies that short waves do not have the small

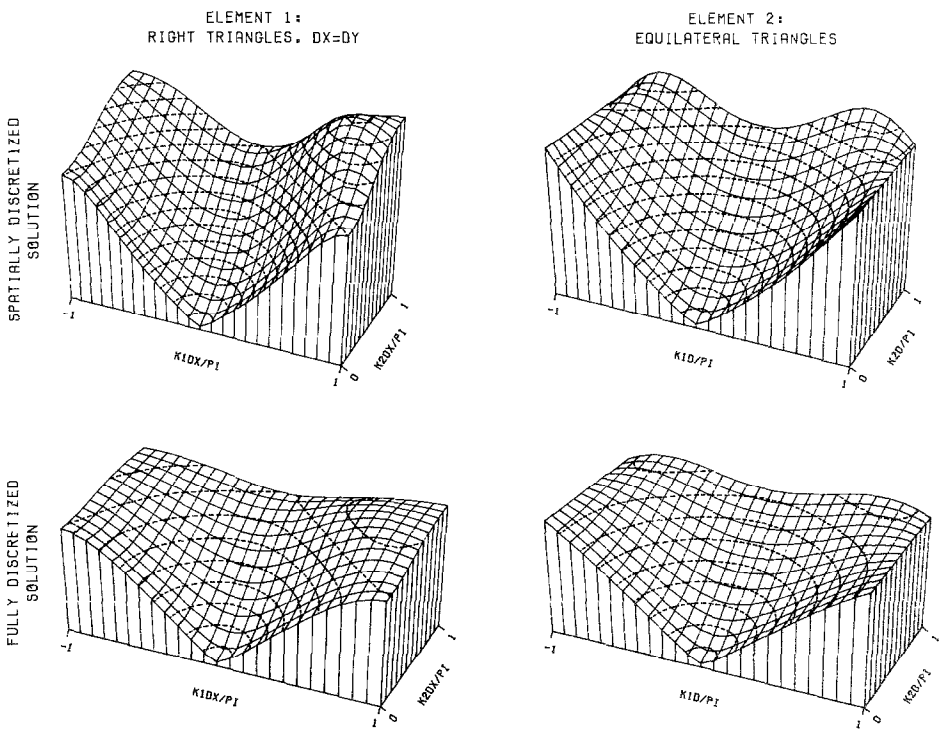

FIG. 10. Dispersion surfaces ($|\omega|\Delta x/(\pi(gh)^{1/2})$) for the WEM. Parameter values are $f_1 = 0.05$, $f_2 = 0.7071$, $f_3 = 0.10$. $\alpha = 1$. $\theta = 0.5$ for element 1 and $\theta = 0.45534$ for element 2. Dotted line contours are in increments of 0.10.

inertial phase velocities (arising from $\omega = f$) discussed in Sections 3 and 4. Provided the parasitic waves do not contaminate the numerical solution, the WEM (with these f_1, f_2, f_3 values) should therefore not have the same short wave problems as the GLFEM and Thacker's method.

The M_A and M_C contours and group velocity vectors corresponding to the dispersion surface plots of Fig. 10 are shown in Fig. 11. High phase velocity accuracy along the axes of element 1 is evident but seems to occur at the expense of accuracy in other directions. For virtually all wavenumbers, element 2 more accurately approximates wave propagation than element 1. And for small wavenumbers, its wave amplitude approximation is also slightly more accurate.

Lynch and Gray [11] also discuss an appropriate quadrature rule which has the effect of lumping their equations. As with Thacker's scheme, this lumping causes all terms of the form $\frac{1}{2}z_0 + \frac{1}{12}(z_1 + z_2 + z_3 + z_4 + z_5 + z_6)$ in the spatially discretized equations to be replaced by z_0. The associated dispersion equation (37) then requires the re-definition $A = 1$. The fully discretized lumped equations, and their associated characteristic equation (39), require these same substitutions. When $\theta = 0$, the LWEM is explicit.

Necessary stability restrictions for the LWEM can also be found when $f = 0$. The parasitic eigenvalues are identical to those for the WEM and are thus governed by the same stability conditions. Similarly, with $A = 1$ substituted in (41), the principal eigenvalues are stable when (43b) is satisfied. These conditions reduce to

$$\theta \geqslant \frac{1}{2}\left(1 - \frac{1}{2f_2^2}\right) \tag{52a}$$

for $\Delta x = \Delta y$ and element 1, and

$$\theta \geqslant \frac{1}{2}\left(1 - \frac{1}{1.47218(f_2')^2}\right) \tag{52b}$$

for the equilateral triangles of element 2.

The LWEM also has values of θ that are most accurate for wave propagation. Assume $f = \tau = 0$. With element 1 and $\Delta x = \Delta y$, the LWEM dispersion relationship is again given by (46a), but

$$D = f_2^2(2 - \cos x - \cos y). \tag{53}$$

Matching the asymptotic dispersion relationship for small x and y with the analytic and setting $y = sx$ now yields

$$\theta = \frac{1}{6}\left[1 - \frac{1 + s^4}{f_2^2(1 + s^2)^2}\right]. \tag{54}$$

As with the WEM, $s = 0$ or $s = \infty$ produces the one-dimensional result [3]

$$\theta = \frac{1}{6}\left(1 - \frac{1}{f_2^2}\right). \tag{55}$$

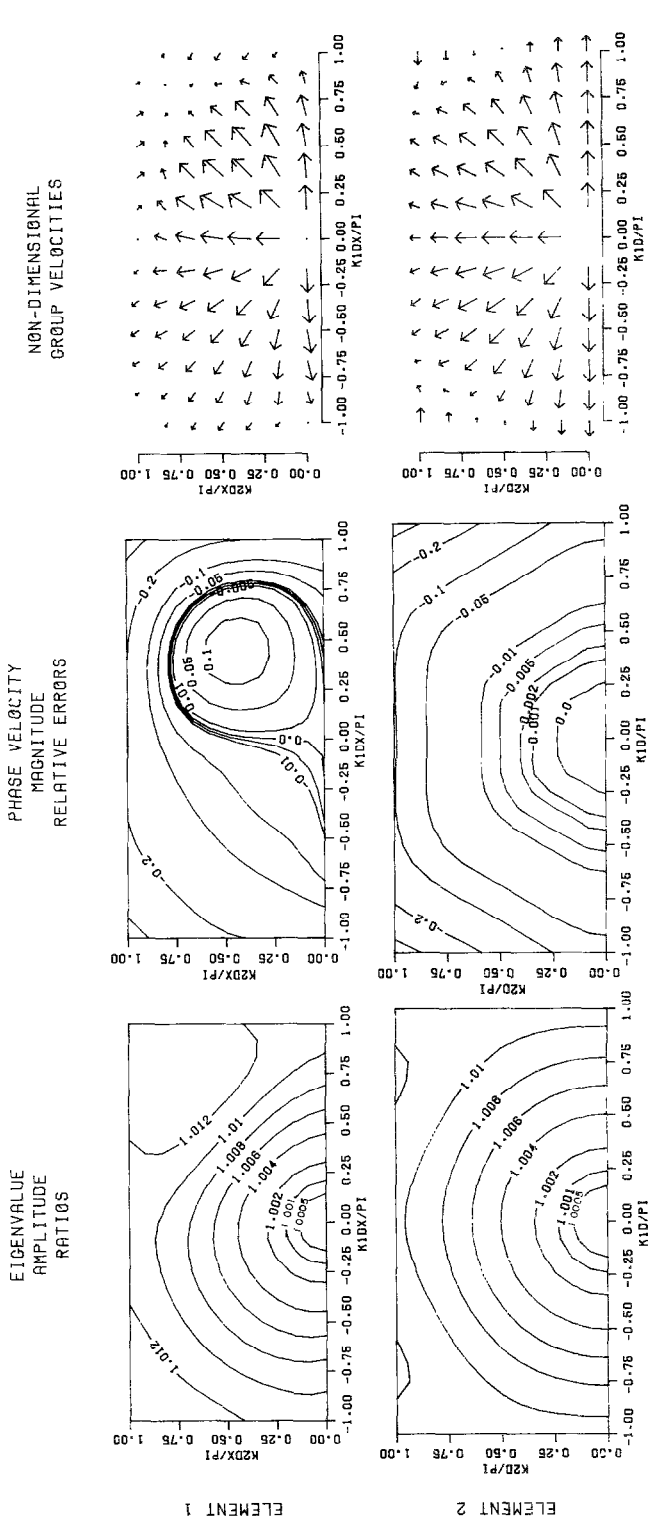

FIG. 11. M_A, M_C, and $\mathbf{G}/(gh)^{1/2}$ for the WEM with the parameter values of Fig. 10.

With $x = k_1 d$, $y = k_2 d$, and $rd = \Delta y$, the LWEM dispersion relationship for element 2 is also given by (46a) but

$$D = (f_2')^2 \left[1 - \cos x + \frac{1}{4}\left(\frac{3}{2} + \frac{1}{2}\cos x - \cos\left(\frac{1}{2} x \right) \cos(ry) \right) \right] \qquad (56)$$

Again, this value is not directionally dependent. And with the substitution $y = ((3)^{1/2}/2)d$, it is identical to the one-dimensional result (55).

In one dimension, $\theta = 0$ produces the most accurate approximation of gravity wave amplitudes for both the WEM and LWEM [3]. The same is true in two dimensions when $f = 0$ and $\tau > 0$. In fact, it is true for both element 1 when $\Delta x = \Delta y$ and the equilateral triangles of element 2. Furthermore, when $f = \tau = 0$, all stable values of θ produce exact amplitudes.

Figure 12 illustrates the stability regions and the most accurate θ values for gravity wave propagation over a configuration of equilateral triangles. Values of f_2' and θ should be chosen so that the resultant numerical method is stable. The particular choice may be a compromise between accuracy and time step size. Large values of Δt (or f_2') result in less computation cost but may be less accurate. Computationally, the explicit LWEM ($\theta = 0$) should be most economical. Unfortunately, the associated f_2' value which most accurately represents phase and group velocity ($f_2' = 0.866025$) is outside the stability region. $f_2' = 0.824175$ is the most accurate and stable choice.

Figure 13 shows the principal dispersion surfaces for the spatially and fully discretized versions of the LWEM. It has the same parameter values, scale, and perspective as Figs. 2, 5, 7, and 10. The time stepping parameters for the fully discretized equations are $\theta = 0$ for element 1 and $\theta = -0.122$ for element 2. The

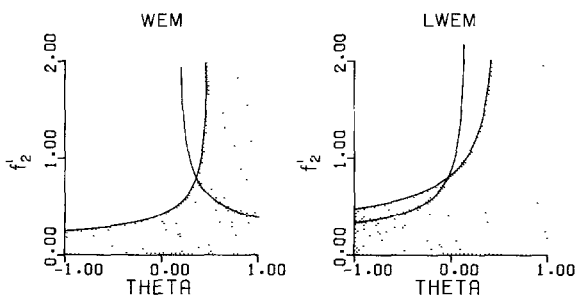

FIG. 12. Stability and accuracy for the WEM and LWEM over equilateral triangles. Shaded regions denote stability. Solid lines designate the most accurate values of θ and f_2' for wave propagation.

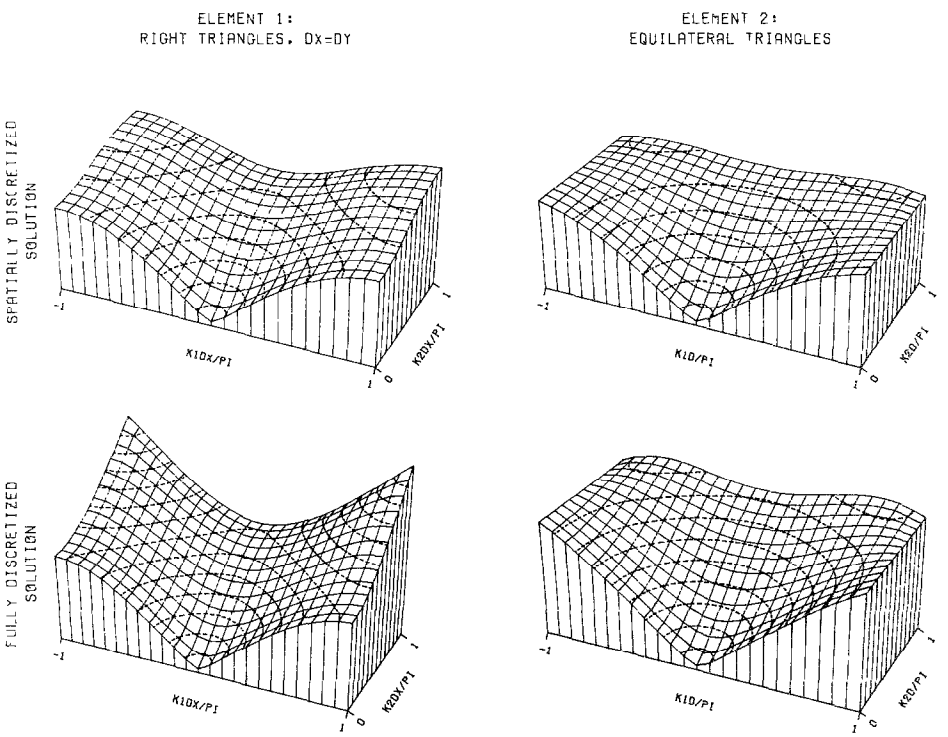

FIG. 13. Dispersion surfaces ($|\omega|\Delta x/(\pi(gh)^{1/2})$) for the LWEM. Parameter values are $f_1 = 0.05$, $f_2 = 0.7071$, $f_3 = 0.10$, $\alpha = 1$, $\theta = 0$ for element 1 and $\theta = -0.122$ for element 2. Dotted line contours are in increments of 0.10.

former is optimal for wave propagation along the directions $y = \pm x$, and as seen from (52a), lies just within the stability limit. (Choosing $\theta = -\frac{1}{6}$, the optimal value for wave propagation along the x or y axis would be unstable.) The θ value for element 2 is optimal for all wave directions and satisfies the stability constraint (52b).

Comparing the spatially discretized surfaces in Figs. 10 and 12, it is evident that lumping has reduced the ω values. However, the chosen time stepping methods are seen to lower the WEM values and raise the LWEM values so that the fully discretized surfaces are more similar.

Figure 14 shows the M_A and M_C contours and the group velocity vectors associated with the dispersion surfaces of Fig. 13. Accurate wave propagation along the lines $x = \pm y$ for element 1 is evident, but appears to be at the expense of accuracy in other directions. For small wavenumbers, element 2 displays the same accuracy in all directions and is generally more accurate than element 1. Wave amplitude accuracy also seems to be independent of direction for element 2. However, it is slightly less accurate than the amplitudes associated with element 1.

The M_C values for element 2 are virtually identical in Fig. 11 and Fig. 14. In fact, with $f_1 = f_3 = 0$, they would be equal. Denoting the optimal parameter values of (51)

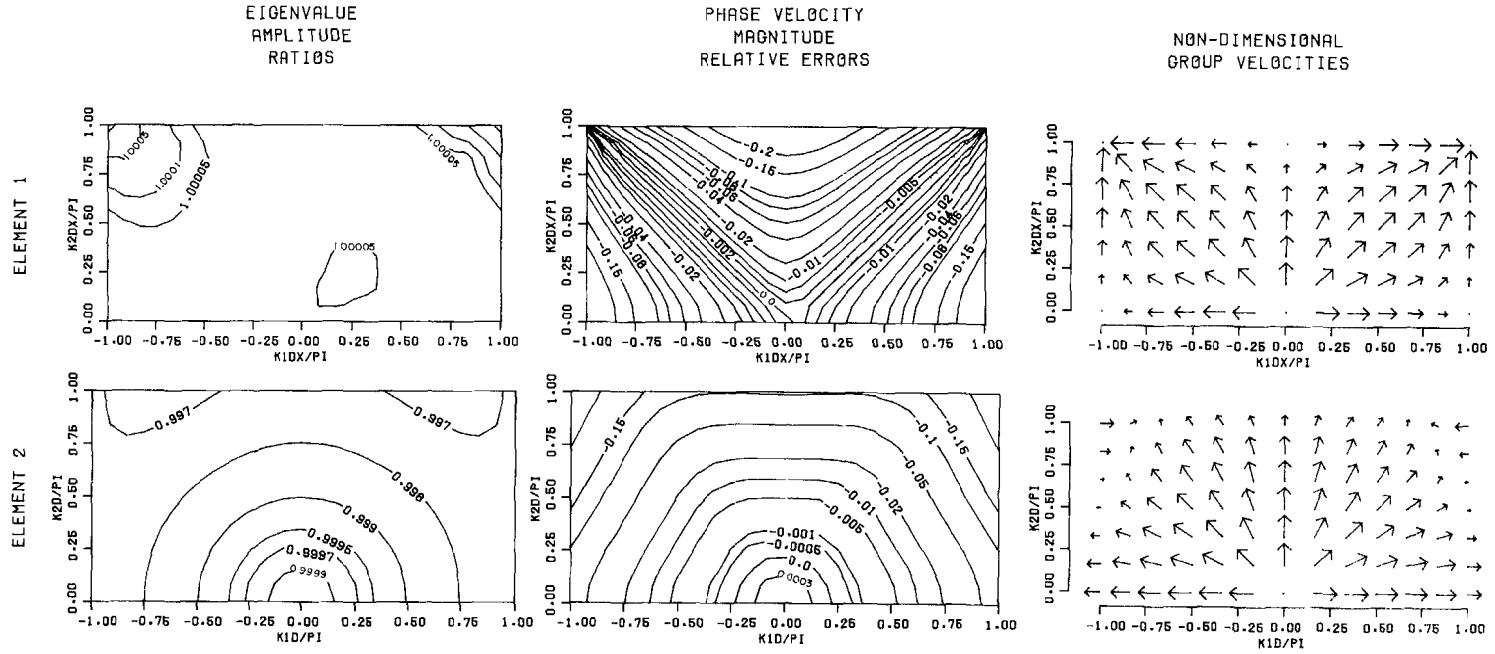

FIG. 14. M_A, M_C, and $G/(gh)^{1/2}$ for the LWEM with the parameter values of Fig. 13.

and (57) by θ^*, the dispersion relationships for both the WEM and LWEM when expanded to terms of order 6 can be expressed as

$$\cos\omega\,\Delta t \simeq 1 - \frac{1}{2}(f_2')^2(x^2+y^2) + \frac{1}{4}(f_2')^4(x^2+y^2)^2\left[\frac{1}{6} + \theta - \theta^*\right]$$
$$- \frac{1}{8}(f_2')^2(x^2+y^2)^3\left[(f_2')^4\left(\theta - \theta^* + \frac{1}{6}\right)^2 - \frac{1}{64}\right]$$
$$- \frac{1}{256}(f_2')^2\left[\frac{11}{45}x^6 + \frac{1}{5}y^6 + x^2y^4 + \frac{1}{3}x^4y^2\right]. \tag{58}$$

This implies that around their respective θ^* values, both the WEM and LWEM have the same accuracy deterioration for $\cos\omega\,\Delta t$. As was found in one dimension, the best time stepping method for the lumped scheme produces the same propagation accuracy (to order 8 in $(k_1 d, k_2 d)$) as the best time stepping method for the unlumped method. Notice that the associated M_A values indicate amplitudes which are too small for the LWEM and too large for the WEM.

6. Comparisons of Accuracy and Economy

Most finite element methods are more expensive than explicit finite difference methods. This is the case with the GLFEM and the RS scheme. This disadvantage is primarily due to the nondiagonal matrix equation which must be solved at each time step. In Sections 4 and 5, it was seen that with explicit time stepping, both Thacker's scheme and the LWEM produce diagonal matrices. Hence they should be much cheaper than the GLFEM. In this section, cost and accuracy comparisons are given for the RS scheme over a square grid, and for Thacker's method and the LWEM over a configuration of equilateral triangles.

Assume identical configurations of equilateral triangles for Thacker's scheme and the LWEM. When $f = \tau = 0$, asymptotic expansions of the nondimensional phase velocity for small $(k_1 d, k_2 d)$ are

$$|\mathbf{C}|/(gh)^{1/2} \simeq 1 + [(k_1 d)^2 + (k_2 d)^2]\left[\frac{1}{24}(f_2')^2 - \frac{1}{8}\right] \tag{59a}$$

$$|\mathbf{C}|/(gh)^{1/2} \simeq 1 + [(k_1 d)^2 + (k_2 d)^2]\left[\frac{1}{24}(f_2')^2 - \frac{1}{32}\right] \tag{59b}$$

for Thacker's scheme and the explicit LWEM, respectively. The associated respective group velocities are

$$\mathbf{G}/(gh)^{1/2} \simeq \left[(k_1^2+k_2^2)^{-1/2} + 3d^2(k_1^2+k_2^2)^{3/2}\left(\frac{1}{24}(f_2')^2 - \frac{1}{8}\right)\right]\mathbf{k} \tag{60a}$$

$$\mathbf{G}/(gh)^{1/2} \simeq \left[(k_1^2+k_2^2)^{-1/2} + 3d^2(k_1^2+k_2^2)^{3/2}\left(\frac{1}{24}(f_2')^2 - \frac{1}{32}\right)\right]\mathbf{k}. \tag{60b}$$

Notice that for high wave resolution, both phase velocities are isotropic and both group velocities have no directional error.

Assuming the optimal stable values for f_2', specifically $f_2' = 1.70437$ for Thacker and $f_2' = 0.824175$ for the LWEM, (59) becomes

$$|\mathbf{C}|/(gh)^{1/2} \simeq 1 - 0.00396345[(k_1 d)^2 + (k_2 d)^2] \tag{61a}$$

$$|\mathbf{C}|/(gh)^{1/2} \simeq 1 - 0.00294732[(k_1 d)^2 + (k_2 d)^2]. \tag{61b}$$

Since the corresponding analytic values are 1.0, the second term in each case is the phase velocity error. Both errors in the group velocity magnitude are larger by a factor of three.

Equation (61) indicates that for identical configurations of equilateral triangles the best explicit LWEM is more accurate than the best Thacker scheme. However, Thacker's scheme is cheaper since it uses a much larger time step. By reducing both d and Δt with Thacker's scheme, it is possible to attain the LWEM accuracy and retain the cost advantage.

If the same accuracy is assumed for both methods, Thacker's Δt becomes larger by the factor 1.78329. However, his smaller d requires 1.34476 more nodes per unit area, and thus more calculations over one time step. The net result is that Thacker's scheme can have the same wave propagation accuracy for small wavenumbers as the LWEM, yet require only 0.75409 the number of calculations per unit area and unit of time.

Despite this cost advantage, Thacker's method may not be preferable to the LWEM. Boundary conditions often introduce short waves into a numerical model. Their accumulation can contaminate the desired longer wave solutions. Problems of this type have been reported with the GLFEM. Since both Thacker's scheme and the GLFEM do not represent short waves accurately, similar problems may also arise with Thacker's scheme. They should not exist with the LWEM.

With $\Delta x = \Delta y$ and $f = \tau = 0$, the RS dispersions relationship is [7]

$$\sin^2(\tfrac{1}{2}\omega\,\Delta t) = f_2^2[\sin^2(\tfrac{1}{2}k_1\,\Delta x) + \sin^2(\tfrac{1}{2}k_2\,\Delta x)]. \tag{62}$$

For small values of $(k_1\,\Delta x, k_2\,\Delta x)$, the asymptotic expansion for the associated nondimensional phase velocity magnitude is

$$|\mathbf{C}|/(gh)^{1/2} \simeq 1 + \frac{1}{24}\left[(f_2^2 - 1)((k_1\,\Delta x)^2 + (k_2\,\Delta x)^2) + \frac{2(k_1\,\Delta x)^2(k_2\,\Delta x)^2}{(k_1\,\Delta x)^2 + (k_2\,\Delta x)^2}\right]. \tag{63}$$

Since it is anisotropic comparisons with (59) are not straightforward.

Let us compare the RS scheme with the LWEM. One grid square of the RS has three unique variables and area Δx^2. One triangular element of the LWEM has area $((3)^{1/2}/4)\,d^2$ and has the equivalent of 1.50 variables, since each node shares its variables with five other triangles. For a comparison based on equal density of the

variables, set $\Delta x = 0.930605d$. Assume the optimal f_2 value (from (63)) when $k_1 = k_2$, namely, $f_2 = (2)^{-1/2}$. Then if $\Delta t'$ is the optimal time step for the LWEM, $\Delta t = 0.79842\Delta t'$ is the optimal time step for the RS. The LWEM is therefore more economical. Its relative accuracy depends on the wave direction. When $k_1 = k_2$, the RS more accurately approximates wave speed. However, when $k_1 = 0$ or $k_2 = 0$, the LWEM is more accurate.

7. Summary and Conclusions

The preceding analysis has demonstrated that finite element methods can be cost competitive and as accurate as explicit finite difference schemes. In particular, Thacker's scheme and the explicit LWEM were found to be cheaper and generally more accurate than the RS finite difference method.

Of the two configurations of triangular elements, the analysis indicates that equilaterial triangles are the better choice. Their phase and group velocities are independent of direction and more accurate for long waves. Numerical tests [8] substantiate this result. In fact, because equilateral triangles seem to produce isotropic waves when the wave resolution is high, they may be the optimal triangular discretization.

Optimal accuracy for Thacker's scheme, the WEM, and the LWEM depends on the parameter f_2'. As discussed in [2], it is both possible and reasonable to keep this parameter approximately constant throughout a model. Consequently, an ideal triangular discretization should employ equilateral triangles whose side length is proportional to $(h)^{1/2}$.

Specific results from the preceding analysis are now summarized by section. The RS scheme studied in Section 2 was found to be quite accurate for small wavenumbers, and for waves travelling at 45° to the grid axes. However, its phase velocity is anisotropic. Asymmetric treatment of the Coriolis terms was also seen to affect the accuracy.

The GLFEM studied in Section 3 displayed accuracy comparable to the RS for small wavenumbers but became very inaccurate at larger wavenumbers. The numerical dispersion surface was seen to have peaks and valleys, implying waves with zero group velocity. Some short waves were calculated to have small inertial speeds while others had group velocities whose directions were incorrect by almost 180°. The configuration of equilateral triangles was found to be more accurate at small wavenumbers than the grid of right triangles.

Thacker's scheme, studied in Section 4, was found to have the same short wave problems as the GLFEM. Stability conditions were calculated for both elements, and the f_2' value which most accurately approximates wave propagation was also calculated. For the equilateral grid, phase velocities were isotropic.

Section 5 included a linear stability analysis when $f = 0$ for both the WEM and the LWEM. An asymptotic analysis for small wavenumbers was also used to determine

the most accurate time stepping method for each scheme. Accuracy was again seen to be directionally dependent with element 1 of Fig. 4, but independent for the equilateral triangles of element 2. It was also shown that with an appropriate time stepping method, wave propagation accuracy can be preserved in going from the WEM to the LWEM.

Section 6 found that for small wavenumbers, the most accurate version of Thacker's scheme can more cheaply attain the same accuracy as the most accurate explicit LWEM. However, Thacker's scheme is less accurate, and may have difficulties, with short waves. The RS scheme was seen to be more expensive per unit of real time than the LWEM. Moreover its accuracy is directionally dependent. For some directions it more accurately models wave propagation than the LWEM, while for other directions it is less accurate.

ACKNOWLEDGMENTS

I thank Professor J. M. Varah and Dr. R. F. Henry for their advice and support throughout this work.

REFERENCES

1. P. B. CREAN, "Hydrodynamics of Estuaries and Fjords" (J. C. J. Nihoul, Ed.), p. 283, Elsevier, Amsterdam, 1978.
2. M. G. G. FOREMAN, *J. Comput. Phys.* **51** (1983), 454.
3. M. G. G. FOREMAN, *J. Comput. Phys.* **52** (1983), 290.
4. W. G. GRAY AND D. R. LYNCH, *Adv. Water Resour.* **1** (1977), 83.
5. W. G. GRAY AND D. R. LYNCH, *Comput. Fluids* **7** (1979), 47.
6. N. S. HEAPS, *Mém. Soc. Roy. Sci. Liège Ser. 6* **2** (1972), 143.
7. R. F. HENRY, *J. Comput. Phys.* **41** (1981), 389.
8. D. E. HINSMAN, R. T. WILLIAMS, AND E. WOODWARD, Recent advances in the Galerkin finite element method as applied to the meteorological equations on variable resolution grids, *in* "Finite Element Flow Analysis" (Tadahiko Kawai, Ed.), University of Tokyo Press, Tokyo, 1982.
9. P. H. LEBLOND AND L. A. MYSAK, "Waves in the Ocean," Elsevier, Amsterdam, 1978.
10. J. LIGHTHILL, "Waves in Fluids," Cambridge Univ. Press, Cambridge, 1978.
11. D. R. LYNCH AND W. G. GRAY, *Comput. Fluids* **7** (1979), 207.
12. F. MESINGER AND A. ARAKAWA, "Numerical Methods Used in Atmospheric Models," Vol. 1, WMO–ICSU Joint Organizing Committee, GARP Publication Series No. 17, 1976.
13. R. MULLEN AND T. BELYTSCHKO, *Internat. J. Numer. Methods Engrg.* **18** (1982), 11.
14. G. F. PINDER AND W. G. GRAY, "Finite Element Simulation in Surface and Subsurface Hydrology," Academic Press, New York, 1977.
15. G. W. PLATZMAN, *Meteorol. Monogr.* **4** (26) (1963).
16. G. W. PLATZMAN, *J. Comput. Phys.* **40** (1981), 36.
17. S. M. SELBY AND B. GIRLING, "Standard Mathematical Tables," Chem. Rubber Co., Cleveland, 1965.
18. A. SIELECKI, *Mon. Weather Rev.* **96** (1968), 150.
19. G. STRANG AND G. J. FIX, "An Analysis of the Finite Element Method," Prentice–Hall, Englewood Cliffs, N.J., 1973.
20. W. C. THACKER, *J. Phys. Oceanogr.* **7** (1977), 284.
21. W. C. THACKER, *J. Phys. Oceanogr.* **8** (1978), 676.

22. W. C. THACKER, *J. Phys. Oceanogr.* **8** (1978), 680.
23. L. N. TREFETHEN, *SIAM Rev.* **24** (1982), 113.
24. R. A. WALTERS AND G. F. CAREY, *Comput. Fluids* **11** (1983), 51.
25. J. D. WANG, *J. Phys. Oceanogr.* **7** (1977), 932.
26. J. D. WANG AND J. J. CONNOR, "Mathematical Modeling of Near Coastal Circulation," MIT Parsons Laboratory Report No. 200, 1975.